

Phenomenology of buoyancy-driven turbulence: recent results

This content has been downloaded from IOPscience. Please scroll down to see the full text.

2017 New J. Phys. 19 025012

(<http://iopscience.iop.org/1367-2630/19/2/025012>)

View [the table of contents for this issue](#), or go to the [journal homepage](#) for more

Download details:

IP Address: 158.144.178.11

This content was downloaded on 11/07/2017 at 06:33

Please note that [terms and conditions apply](#).

You may also be interested in:

[Energy Spectra in Rayleigh-Benard Convection](#)

Mahendra K Verma, Pankaj Mishra, Mani Chandra et al.

[Anisotropy in Quasi-Static Magnetohydrodynamic Turbulence](#)

Mahendra K Verma

[TURBULENT TRANSPORT IN A STRONGLY STRATIFIED FORCED SHEAR LAYER WITH THERMAL](#)

[DISPERSION](#)
Hussein Aluie and Logithan Kulenthirajah

[Coarse-grained incompressible magnetohydrodynamics: analyzing the turbulent cascades](#)

Hussein Aluie

[On flow reversals in Rayleigh-Bénard convection](#)

Mani Chandra and Mahendra K Verma

[Transient effects in unstable ablation fronts and mixing layers in HEDP](#)

J-M Clarisse, S Gauthier, L Dastugue et al.

[Heat transfer in cryogenic helium gas by turbulent Rayleigh-Bénard convection in a cylindrical cell of aspect ratio 1](#)

Pavel Urban, Pavel Hanzelka, Vra Musilová et al.

[Energy transfer and bottleneck effect in turbulence](#)

Mahendra K Verma and Diego Donzis

[Numerical Modeling of Solar Tachocline. II.](#)

Mark S. Miesch



PAPER

Phenomenology of buoyancy-driven turbulence: recent results

OPEN ACCESS

RECEIVED
27 October 2016REVISED
24 December 2016ACCEPTED FOR PUBLICATION
1 February 2017PUBLISHED
27 February 2017Original content from this work may be used under the terms of the [Creative Commons Attribution 3.0 licence](#).

Any further distribution of this work must maintain attribution to the author(s) and the title of the work, journal citation and DOI.



Mahendra K Verma, Abhishek Kumar and Ambrish Pandey

Department of Physics, Indian Institute of Technology Kanpur, Kanpur 208016, India

E-mail: mkv@iitk.ac.in**Keywords:** buoyancy-driven flows, Rayleigh–Bénard convection, stably-stratified turbulence, thermal convection, thermally-driven turbulence

Abstract

In this paper, we describe the recent developments in the field of buoyancy-driven turbulence with a focus on energy spectrum and flux. Scaling and numerical arguments show that the stably-stratified turbulence with moderate stratification has kinetic energy spectrum $E_u(k) \sim k^{-11/5}$ and the kinetic energy flux $\Pi_u(k) \sim k^{-4/5}$, which is called Bolgiano–Obukhov scaling. However, for Prandtl number near unity, the energy flux for the three-dimensional Rayleigh–Bénard convection (RBC) is approximately constant in the inertial range that results in Kolmogorov’s spectrum ($E_u(k) \sim k^{-5/3}$) for the kinetic energy. The phenomenology of RBC should apply to other flows where the buoyancy feeds the kinetic energy, e.g. bubbly turbulence and fully-developed Rayleigh Taylor instability. This paper also covers several models that predict the Reynolds and Nusselt numbers of RBC. Recent works show that the viscous dissipation rate of RBC scales as $\sim Ra^{1.3}$, where Ra is the Rayleigh number.

1. Introduction

Gravity pervades the whole universe, and it plays a dominant role in the flow dynamics of the interiors and atmospheres of planets and stars. The gravitational force also affects the engineering flow, e.g., in large turbines. Therefore, understanding the physics of buoyancy-driven turbulence is quite crucial.

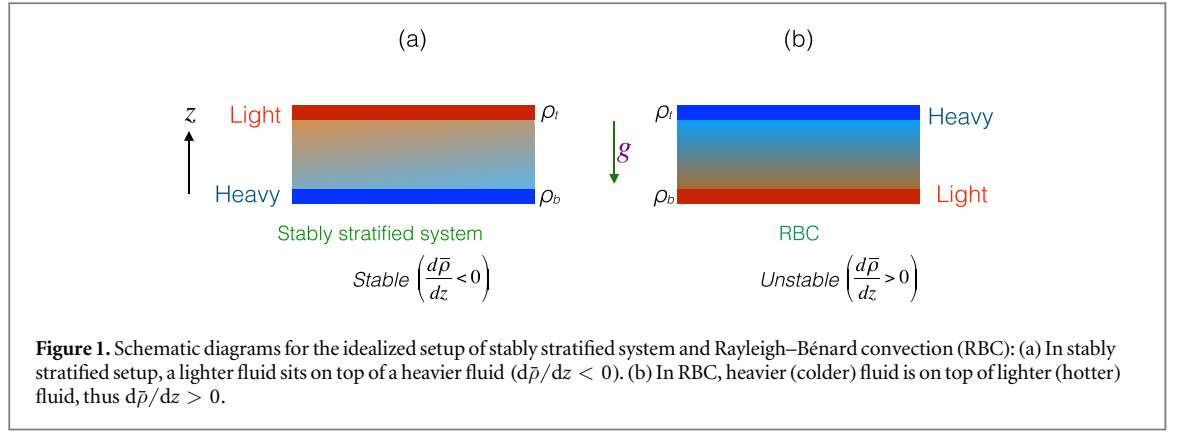
Hydrodynamic turbulence is described quite well by Kolmogorov’s theory [50] according to which the energy spectrum ($E(k)$) in the inertial range is described by

$$E(k) = K_{Ko} \Pi^{2/3} k^{-5/3}, \quad (1)$$

where K_{Ko} is the Kolmogorov’s constant, and Π is the energy flux or energy cascade rate, which is assumed to be constant in the inertial range. In Kolmogorov’s phenomenology for hydrodynamic turbulence, the flow is forced at large length scales. However in buoyancy-driven flows, the buoyancy provides forcing at all length scales, hence the kinetic energy flux Π_u is expected to be a function of wavenumber k . Bolgiano [11] and Obukhov [81] exploited this idea to derive energy spectrum for stably-stratified turbulence (SST); their scaling arguments yield $\Pi_u(k) \sim k^{-4/5}$, and the kinetic energy spectrum $E_u(k) \sim k^{-11/5}$. Here the kinetic energy is converted to potential energy that leads to decrease of $\Pi(k)$ with k . Procaccia and Zeitak [89], L’vov [65], L’vov and Falkovich [66], and Rubinstein [91] argued that the scaling of Bolgiano [11] and Obukhov [81] would extend to the thermally-driven turbulence as well. Kumar *et al* [53] however showed that in turbulent convection, the buoyancy feeds the kinetic energy, hence $\Pi_u(k)$ cannot decrease with k , and Bolgiano–Obukhov’s arguments are not valid for thermally-driven turbulence. Using a detailed analysis, Kumar *et al* [53] showed that turbulent thermal convection shows Kolmogorov’s $k^{-5/3}$ energy spectrum.

Strong gravity makes the flow anisotropic. Surprisingly the turbulent flow in Rayleigh–Bénard convection (RBC) is nearly isotropic [75], while the SST is nearly isotropic when Richardson number is less than unity [53]. The stably-stratified flows become quasi two-dimensional for larger Richardson numbers. For RBC the large-scale quantities like Reynolds and Nusselt numbers exhibit interesting scaling relations.

In this paper we describe the recent results of the field, with focus on spectral properties of buoyancy-driven turbulence. Refer to the review articles [2, 8, 29, 63, 98] for more comprehensive discussion on various topics of RBC. We introduce the governing equation and system description in section 2. We cover recent development



on energy spectrum and flux in section 3, and scaling of large-scale quantities in section 4. Section 5 contains a brief description of the dynamics of flow reversal. We conclude in section 6.

2. System description

In this section we describe the the buoyancy-driven systems and their associated equations.

2.1. Equations under Oberbeck–Boussinesq approximation

Consider fluid between two layers separated by distance d with the bottom density at ρ_b and the top density at ρ_t (see figure 1). Clearly the fluid is under the influence of an external density stratification. Under equilibrium condition, the density profile is

$$\bar{\rho}(z) = \rho_b + \frac{d\bar{\rho}}{dz}z = \rho_b + \frac{\rho_t - \rho_b}{d}z. \quad (2)$$

We denote $\bar{\rho}(z)$ as the mean density profile. With fluctuations, the local density ρ_l (subscript l stands for local) is

$$\rho_l(x, y, z) = \bar{\rho} + \rho(x, y, z). \quad (3)$$

The gravitational force on a unit volume is $-\rho_l g \hat{z}$, where $-g \hat{z}$ is the acceleration due to gravity. Hence the gravitational force density on the fluid is

$$\mathbf{F}_g = -g \rho_l \hat{z} = -g(\bar{\rho} + \rho) \hat{z} = -g \nabla \left(\int^z \bar{\rho}(z') dz' \right) - \rho g \hat{z}. \quad (4)$$

The force $\rho g \hat{z}$ occurring due to the change in density from the local value is the *buoyancy*. It is along $-\hat{z}$ (downward) for $\rho > 0$, but along \hat{z} (upward) for $\rho < 0$ (see figure 1).

The fluid flow is described by the Navier–Stokes equation

$$\rho_l \left[\frac{\partial \mathbf{u}}{\partial t} + (\mathbf{u} \cdot \nabla) \mathbf{u} \right] = -\nabla p + \mathbf{F}_g + \mu \nabla^2 \mathbf{u} + \mathbf{f}_u, \quad (5)$$

where \mathbf{u} , p are the velocity and pressure fields respectively, μ is the dynamic viscosity of the fluid, and \mathbf{f}_u is the external force in addition to the buoyancy. Substitution of equation (4) in equation (5) yields

$$\rho_l \left[\frac{\partial \mathbf{u}}{\partial t} + (\mathbf{u} \cdot \nabla) \mathbf{u} \right] = -\nabla \sigma - \rho g \hat{z} + \mu \nabla^2 \mathbf{u}, \quad (6)$$

where

$$\sigma = p + g \int^z \bar{\rho}(z') dz' \quad (7)$$

is the modified pressure.

The continuity equation for the density is

$$\frac{\partial \rho_l}{\partial t} + \nabla \cdot (\rho_l \mathbf{u}) = \nabla \cdot (\kappa \nabla \rho_l), \quad (8)$$

where κ is the diffusivity of the density. We assume that κ is constant in space and time. We can rewrite equation (8) as

$$\nabla \cdot \mathbf{u} = -\frac{1}{\rho_l} \frac{d\rho_l}{dt} + \frac{1}{\rho_l} \kappa \nabla^2 \rho_l. \quad (9)$$

Now we employ Oberbeck–Boussinesq approximation according to which $(d\rho_l/dt)/\rho_l \approx 0$. Hence the relative magnitude of $\nabla \cdot \mathbf{u}$ is

$$\frac{\nabla \cdot \mathbf{u}}{U/L} \approx \frac{L}{\rho_l U} \kappa \nabla^2 \rho_l \approx \frac{\kappa}{UL} = \frac{1}{\text{Pe}}, \quad (10)$$

where L , U are the large length and velocity scales respectively, and Pe is the Péclet number. Hence for large Pe , which is often the case for buoyancy-driven flows, we can assume that $\nabla \cdot \mathbf{u} = 0$. Therefore, under the Oberbeck–Boussinesq approximation, equation (8) gets simplified. In addition, we replace ρ_l of equation (6) with the mean density of the fluid, ρ_m . Hence the governing equations for the buoyancy-driven flows are

$$\frac{\partial \mathbf{u}}{\partial t} + (\mathbf{u} \cdot \nabla) \mathbf{u} = -\frac{1}{\rho_m} \nabla \sigma - \frac{\rho}{\rho_m} g \hat{z} + \nu \nabla^2 \mathbf{u} + \mathbf{f}_u, \quad (11)$$

$$\frac{\partial \rho}{\partial t} + (\mathbf{u} \cdot \nabla) \rho = -\frac{d\bar{\rho}}{dz} u_z + \kappa \nabla^2 \rho, \quad (12)$$

where $\nu = \mu/\rho_m$ is the kinematic viscosity. The assumption that ν , κ are constants in space and time is also considered to be a part of the Oberbeck–Boussinesq approximation. Also note that the buoyancy term, which is a function of variable density, is retained in the Navier–Stokes equation since it is comparable to the other terms of the momentum equation (see section 2.9). In the SST, the total energy decays without \mathbf{f}_u , hence \mathbf{f}_u is employed to maintain a steady state.

Note that the system is stable when heavy fluid is below the lighter fluid, or $d\bar{\rho}/dz < 0$ (see figure 1(a)). Such systems yield wave solution in the linear limit. On the contrary, when heavy fluid is above the lighter fluid, $d\bar{\rho}/dz > 0$ and the flow becomes unstable and convective (see figure 1(b)).

Temperature field T induces density variation in the following manner:

$$\rho_l = \rho_b [1 - \alpha(T - T_b)], \quad (13)$$

where α is the thermal expansion coefficient, which is assumed to be constant in space and time. Hence we can rewrite equations (11), (12) in terms of the temperature field. Let us consider a fluid confined between two thermally-conducting horizontal plates kept at constant temperatures, as shown in figure 1(b). We denote the temperatures of the bottom and top plates to be T_b and T_t respectively, and $\Delta = T_b - T_t$.

Thermal convection is absent for small Δ . Under this condition, the temperature profile is linear as

$$\bar{T}(z) = T_b + \frac{d\bar{T}}{dz} z = T_b - \frac{T_b - T_t}{d} z, \quad (14)$$

and the heat is transported by conduction. This configuration has no fluctuation, i.e., $\mathbf{u} = 0$ and $\rho = 0$. The flow however becomes unstable and convective when Δ exceeds a certain critical value. For such flows it is customary to write the temperature as

$$T(x, y, z) = \bar{T}(z) + \theta(x, y, z), \quad (15)$$

where θ is the temperature fluctuation over the background conduction profile \bar{T} . The equations (3), (13), (15) yield

$$\rho = -\rho_m \alpha \theta; \quad \frac{d\bar{\rho}}{dz} = -\alpha \frac{d\bar{T}}{dz}, \quad (16)$$

substitution of which in equations (11), (12) yields the following set of governing equations:

$$\frac{\partial \mathbf{u}}{\partial t} + (\mathbf{u} \cdot \nabla) \mathbf{u} = -\frac{1}{\rho_m} \nabla \sigma + \alpha g \theta \hat{z} + \nu \nabla^2 \mathbf{u}, \quad (17)$$

$$\frac{\partial \theta}{\partial t} + (\mathbf{u} \cdot \nabla) \theta = -\frac{d\bar{T}}{dz} u_z + \kappa \nabla^2 \theta, \quad (18)$$

$$\nabla \cdot \mathbf{u} = 0. \quad (19)$$

The above fluid configuration under Oberbeck–Boussinesq approximation is called RBC. The flow dynamics of RBC is described by equations (17)–(19).

2.2. Nondimensionalized equations

Fluid flows are conveniently described by nondimensional equations since they capture relative strengths of various terms of the equations. Also, they help reduce the number of parameters of the system, which is quite useful for analysis, as well as for the numerical simulations and experiments. Equations (11), (12) have been nondimensionalized in various ways. Here, we present two such schemes. When we use d as the length scale,

κ/d as the velocity scale, d^2/κ as the time scale, and $\Delta\rho = |\rho_b - \rho_t|$ as the density scale, we obtain the following nondimensional equations:

$$\frac{\partial \mathbf{u}}{\partial t} + (\mathbf{u} \cdot \nabla) \mathbf{u} = -\nabla \sigma - \text{Ra Pr} \rho \hat{z} + \text{Pr} \nabla^2 \mathbf{u}, \quad (20)$$

$$\frac{\partial \rho}{\partial t} + (\mathbf{u} \cdot \nabla) \rho = -S u_z + \nabla^2 \rho, \quad (21)$$

where $\rho \rightarrow \rho/(\Delta\rho)$, and

$$\text{Prandtl number } \text{Pr} = \frac{\nu}{\kappa}, \quad (22)$$

$$\text{Rayleigh number } \text{Ra} = \frac{g d^3 \Delta\rho}{\nu \kappa \rho_m}, \quad (23)$$

$$\text{Normalized density gradient } S = \frac{d}{\Delta\rho} \frac{d\bar{\rho}}{dz}. \quad (24)$$

For the stably-stratified flows, $S = -1$, but $S = 1$ for RBC. Using equation (16) we can write the above equation in terms of temperature field as follows:

$$\frac{\partial \mathbf{u}}{\partial t} + (\mathbf{u} \cdot \nabla) \mathbf{u} = -\nabla \sigma + \text{Ra Pr} \theta \hat{z} + \text{Pr} \nabla^2 \mathbf{u} \quad (25)$$

$$\frac{\partial \theta}{\partial t} + (\mathbf{u} \cdot \nabla) \theta = S u_z + \nabla^2 \theta, \quad (26)$$

for which

$$\text{Ra} = \frac{\alpha g \Delta d^3}{\nu \kappa}, \quad (27)$$

where Δ is the temperature difference between the bottom and top plates, as defined earlier. Note however that for large Ra, the aforementioned nondimensional velocity becomes very large ($\sim \sqrt{\text{Ra Pr}}$) [38, 116] that becomes an obstacle for numerical simulations due to very small time-steps. Hence, in numerical simulations, it is customary to employ $\sqrt{\alpha g \Delta d}$ as the velocity scale, which yields the following set of equations:

$$\frac{\partial \mathbf{u}}{\partial t} + (\mathbf{u} \cdot \nabla) \mathbf{u} = -\nabla \sigma + \theta \hat{z} + \sqrt{\frac{\text{Pr}}{\text{Ra}}} \nabla^2 \mathbf{u}, \quad (28)$$

$$\frac{\partial \theta}{\partial t} + (\mathbf{u} \cdot \nabla) \theta = S u_z + \frac{1}{\sqrt{\text{Ra Pr}}} \nabla^2 \theta. \quad (29)$$

For stably-stratified flows, researchers often employ dimensional equations, but with density converted to units of velocity by a transformation [61]

$$b = \frac{g}{N} \frac{\rho}{\rho_m}, \quad (30)$$

where

$$N = \sqrt{\frac{g}{\rho_m} \left| \frac{d\bar{\rho}}{dz} \right|} \quad (31)$$

is the Brunt-Väisälä frequency. In terms of the above variables, the equations become

$$\frac{\partial \mathbf{u}}{\partial t} + (\mathbf{u} \cdot \nabla) \mathbf{u} = -\nabla \sigma - N b \hat{z} + \nu \nabla^2 \mathbf{u}, \quad (32)$$

$$\frac{\partial b}{\partial t} + (\mathbf{u} \cdot \nabla) b = N u_z + \kappa \nabla^2 b. \quad (33)$$

The other important nondimensional parameters used for describing the buoyancy-driven flows are

$$\text{Reynolds number } \text{Re} = \frac{u_{\text{rms}} d}{\nu}, \quad (34)$$

$$\text{Froude number } \text{Fr} = \frac{u_{\text{rms}}}{d N}, \quad (35)$$

$$\text{Richardson number } \text{Ri} = \frac{N b_{\text{rms}}}{u_{\text{rms}}^2 / d} = \frac{1}{\text{Fr}^2}, \quad (36)$$

where u_{rms} , b_{rms} are respectively the rms velocity and the rms value of b . Note that the Richardson number is the ratio of the buoyancy and the nonlinearity $(\mathbf{u} \cdot \nabla) \mathbf{u}$. Another important nondimensional parameter for RBC is

the Nusselt number Nu, which is the ratio of the total heat flux (convective plus conductive) and the conductive heat flux, and is computed using the following formula:

$$\text{Nu} = \frac{\kappa\Delta/d + \langle u_z\theta \rangle}{\kappa\Delta/d}. \quad (37)$$

2.3. Boundary conditions

For the velocity field we employ the following set of boundary conditions:

- (i) No-slip: All the components of the velocity field vanish at the walls, i.e., $\mathbf{u} = 0$.
- (ii) Free-slip: At a wall, the normal component of the velocity field vanishes, i.e., $\mathbf{u} \cdot \hat{n} = 0$, and the gradient of the parallel components of the velocity vanishes, i.e., $\partial u_{\parallel}/\partial n = 0$.
- (iii) Periodic: The velocity is periodic, i.e., $\mathbf{u}(\mathbf{x} + lL_x\hat{x} + mL_y\hat{y} + nL_z\hat{z}) = \mathbf{u}(\mathbf{x})$, where l, m, n are integers, and the box is of the size $L_x \times L_y \times L_z$.

For the temperature field, the typical boundary condition used are

- (i) Conducting: Uniform temperature field at the walls, i.e., $\theta = 0$.
- (ii) Insulating: The temperature flux at the wall is zero, i.e., $\partial\theta/\partial n = 0$.
- (iii) Periodic: The temperature fluctuation is periodic, i.e., $\theta(\mathbf{x} + lL_x\hat{x} + mL_y\hat{y} + nL_z\hat{z}) = \theta(\mathbf{x})$.

2.4. Exact relations

Equations (11), (12) are nonlinear, and hence researchers have not been able to write down general analytic solutions for them. However, Shraiman and Siggia [97] derived the following exact relations of the viscous dissipation rate (ϵ_u) and the thermal dissipation rate (ϵ_T) for RBC flows:

$$\epsilon_u = \nu \langle \omega^2 \rangle = \frac{\nu^3 (\text{Nu} - 1) \text{Ra}}{d^4 \text{Pr}^2}, \quad (38)$$

$$\epsilon_T = \kappa \langle (\nabla T)^2 \rangle = \kappa \frac{\Delta^2}{d^2} \text{Nu}, \quad (39)$$

where $\boldsymbol{\omega} = \nabla \times \mathbf{u}$. Also, in the idealized limit of $\nu = \kappa = 0$, using equations (32), (33), we deduce that the total energy

$$E = \frac{1}{2} \int (u^2 \pm b^2) d\mathbf{r} \quad (40)$$

is conserved for periodic and vanishing boundary conditions. In the above, the positive sign is for the stably-stratified flow, while the negative sign for the RBC. A stably-stratified flow is stable, for which the $u^2/2$ and $b^2/2$ terms are the kinetic and potential energies respectively, analogous to a harmonic oscillator. In RBC, the conserved quantity is also written as $\int [u^2 - \alpha g \theta^2 / (d\bar{T}/dz)] / 2 d\mathbf{r}$, where $\theta^2/2$ is called *entropy*. Note that $\theta^2/2$ is not the thermodynamic entropy that quantifies the degree of disorder at the microscopic scales.

It is convenient to describe behaviour of turbulent flows in spectral or Fourier space since it captures the scale-by-scale energy and interactions quite well. In the next subsection, we describe the definitions used for such descriptions.

2.5. Equations in Fourier space

We rewrite equations (17)–(19) in the Fourier space as

$$\left(\frac{d}{dt} + \nu k^2 \right) u_i(\mathbf{k}, t) = -ik_i \frac{\sigma(\mathbf{k}, t)}{\rho_m} - ik_j \sum_{\mathbf{k}=\mathbf{p}+\mathbf{q}} u_j(\mathbf{q}, t) u_i(\mathbf{p}, t) + \alpha g \theta(\mathbf{k}, t) \hat{z}, \quad (41)$$

$$\left(\frac{d}{dt} + \kappa k^2 \right) \theta(\mathbf{k}, t) = -\frac{d\bar{T}}{dz} \hat{u}_z(\mathbf{k}, t) - ik_j \sum_{\mathbf{k}=\mathbf{p}+\mathbf{q}} u_j(\mathbf{q}, t) \theta(\mathbf{p}, t), \quad (42)$$

$$k_i u_i(\mathbf{k}, t) = 0. \quad (43)$$

In the above equations, i represents two things: $\sqrt{-1}$ in front of the $k_i \sigma(\mathbf{k}, t) / \rho_m$ term, and $i = x, y, z$ in u_i . Note that $\mathbf{u}(k)$, $\sigma(\mathbf{k})$, and $\theta(\mathbf{k})$ are the Fourier transforms of \mathbf{u} , σ , and θ , respectively. The above equations are in terms of θ , but we can easily convert them as a function of ρ .

In the Fourier space, $E_u(k)$ denotes the kinetic energy spectrum, which is the sum of the kinetic energies of all the modes in a given shell $(k - 1, k]$. Similarly we define the spectra for the entropy and potential energy, which are denoted by $E_\theta(k)$ and $E_b(k)$ respectively. They are computed using the following formulas:

$$E_u(k) = \sum_{k-1 < k' \leq k} \frac{1}{2} |\mathbf{u}(\mathbf{k}')|^2, \quad (44)$$

$$E_\theta(k) = \sum_{k-1 < k' \leq k} \frac{1}{2} |\theta(\mathbf{k}')|^2, \quad (45)$$

$$E_b(k) = \sum_{k-1 < k' \leq k} \frac{1}{2} |b(\mathbf{k}')|^2. \quad (46)$$

2.6. Linear and nonlinear regimes

The behavior of buoyancy driven flows depends on the parameters and dimensionality. Here we present a bird's-eye view of the observed states of RBC and stably-stratified flows.

2.6.1. RBC

It can be easily shown that equations (25), (26) yield a unstable solution at $Ra = Ra_c$, with $Ra_c = 27\pi^4/4$ for the free-slip boundary condition, and $Ra_c \approx 1708$ for the no-slip boundary condition [23]. The unstable solutions are the convective rolls. For Ra just above the onset, the instability saturates due to nonlinearity leading to the *roll* solutions. At larger Ra , the nonlinearity yields patterns and chaos [5, 17, 23, 67, 73, 83]. For even larger nonlinearity, spatio-temporal chaos, weak turbulence, and strong turbulence emerge [67]. In this paper we will focus on only the strong turbulence regime.

2.6.2. Stably-stratified flow

For $S = -1$, the linearised version of equations (20), (21) yields internal gravity waves whose dispersion relation is

$$\omega = \frac{k_\perp}{k} N, \quad (47)$$

where $k_\perp = \sqrt{k_x^2 + k_y^2}$ is the wavenumber component perpendicular to the buoyancy direction. Clearly $\omega = N$ for $k_\parallel = 0$. These internal gravity waves persist for weak nonlinearity and inviscid case ($\nu = \kappa = 0$). Strong nonlinearity has two kinds of generic behaviour: Strong stratification ($Fr \ll 1$) suppresses the flow along the buoyancy direction and yields a quasi two-dimensional (2D) stratified flow; on the other hand, moderate and weak stratification ($Fr \gtrsim 1$) yields near isotropic turbulent flows. For $Fr \approx 1$, Kumar *et al* [53] obtained Bolgiano-Obukhov [11, 81] scaling as predicted (to be described in section 3.3.1). In this paper we focus on the $Fr \gtrsim 1$ regime.

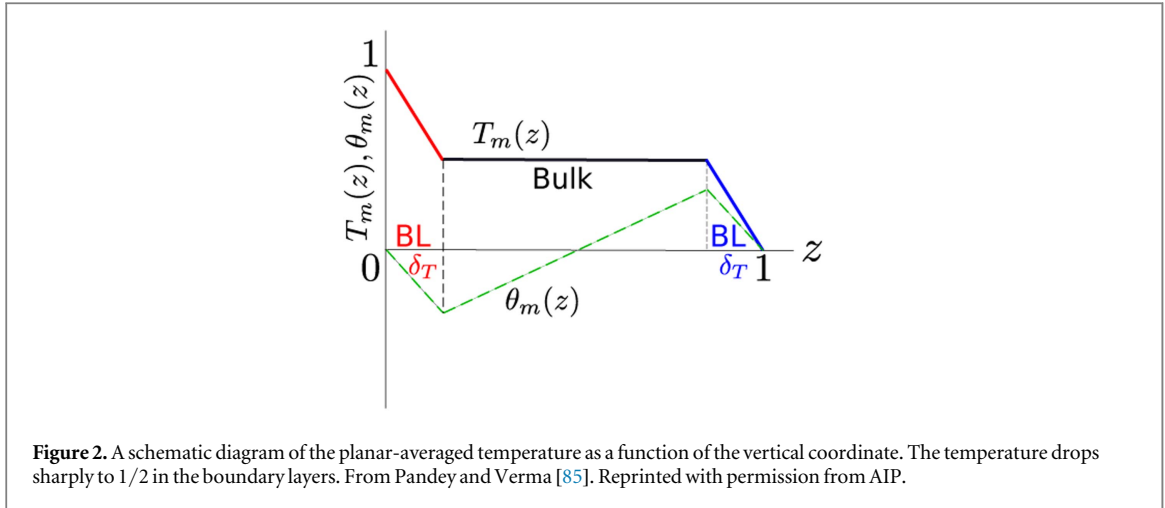
2.7. Temperature profile and related equations

In this subsection we derive the properties of temperature fluctuations of RBC. For convenience we work with nondimensional variables.

Experiments and numerical simulations of RBC reveal that the horizontally averaged temperature $T_m(z)$ remains approximately a constant ($\approx 1/2$) in the bulk, and its value drops sharply in the thermal boundary layers [34, 95], as shown in figure 2. The quantitative expression for $T_m(z) = \langle T \rangle_{xy}$ can be approximated as

$$T_m(z) = \begin{cases} 1 - \frac{z}{2\delta_T} & \text{for } 0 < z < \delta_T, \\ 1/2 & \text{for } \delta_T < z < 1 - \delta_T, \\ \frac{1-z}{2\delta_T} & \text{for } 1 - \delta_T < z < 1, \end{cases} \quad (48)$$

where δ_T is the thickness of the thermal boundary layer, and $\langle \rangle_{xy}$ represents averaging over the xy planes. A horizontal averaging of equation (15) yields $\theta_m(z) = T_m(z) + z - 1$, and hence $\theta_m(z)$ is



$$\theta_m(z) = \begin{cases} z \left(1 - \frac{1}{2\delta_T}\right) & \text{for } 0 < z < \delta_T \\ z - 1/2 & \text{for } \delta_T < z < 1 - \delta_T \\ (z - 1) \left(1 - \frac{1}{2\delta_T}\right) & \text{for } 1 - \delta_T < z < 1 \end{cases} \quad (49)$$

as exhibited in figure 2. For thin thermal boundary layers, $\theta_m(0, 0, k_z)$, which is the Fourier transform of $\theta_m(z)$, is dominated by the contributions from the bulk. Hence

$$\begin{aligned} \theta_m(0, 0, k_z) &= \int_0^1 \theta_m(z) \sin(k_z \pi z) dz \\ &\approx \int_0^1 (z - 1/2) \sin(k_z \pi z) dz \\ &\approx \begin{cases} -\frac{1}{\pi k_z} & \text{for even } k_z \\ 0 & \text{otherwise.} \end{cases} \end{aligned} \quad (50)$$

The corresponding velocity mode, $u_z(0, 0, k_z) = 0$ because of the incompressibility condition $\mathbf{k} \cdot \mathbf{u}(0, 0, k_z) = k_z u_z(0, 0, k_z) = 0$. Also, $u_x(0, 0, k_z) = u_y(0, 0, k_z) = 0$ in the absence of a mean flow along the horizontal direction. Hence for the $\mathbf{k} = (0, 0, k_z)$ modes, the momentum equation yields

$$0 = -\frac{\mathbf{k}\sigma(\mathbf{k})}{\rho_0} + \alpha g \theta(\mathbf{k}) \hat{\mathbf{z}} \quad (51)$$

or $d\sigma_m(z)/dz = \rho_0 \alpha g \theta_m$, and the dynamics of the remaining set of Fourier modes is governed by the momentum equation as

$$\frac{\partial \mathbf{u}(\mathbf{k})}{\partial t} + \mathbf{i} \sum_{\mathbf{p}+\mathbf{q}=\mathbf{k}} [\mathbf{k} \cdot \mathbf{u}(\mathbf{q})] \mathbf{u}(\mathbf{p}) = -\frac{\mathbf{k}\sigma_{\text{res}}(\mathbf{k})}{\rho_0} + \alpha g \theta_{\text{res}}(\mathbf{k}) \hat{\mathbf{z}} - \nu k^2 \hat{\mathbf{u}}(\mathbf{k}), \quad (52)$$

where

$$\theta = \theta_{\text{res}} + \theta_m; \quad \sigma = \sigma_{\text{res}} + \sigma_m. \quad (53)$$

Hence, the modes $\theta_m(0, 0, k_z)$ and $\sigma_m(0, 0, k_z)$ do not couple with the velocity modes in the momentum equation, but θ_{res} and σ_{res} do.

Equation (52) has strong implications on the scaling of the Reynolds and Nusselt numbers, which will be discussed in section 4. In addition, the set of Fourier modes $\theta(0, 0, k_z)$ of equation (50) yields $E_\theta(k) \sim k^{-2}$. This issue will be discussed in section 3.

2.8. Other related systems

Several buoyancy-driven systems can be related to RBC. Here we list some of these systems.

2.8.1. Rayleigh–Taylor instability (RTI)

A fluid configuration with a denser fluid above a lighter fluid is unstable. The heavier fluid falls and the lighter fluid rises. After an initial stage of RTI, the flow develops significant nonlinearity and becomes turbulent [24]. We will discuss later that the turbulence phenomenology of RTI is similar to that of RBC.

2.8.2. Taylor–Couette flow

Two coaxial rotating cylinders create random flow at large Taylor number. This flow has been related to RBC with significant similarities in their phenomenology. See Grossmann *et al* [43] for a review of such flows.

2.8.3. Turbulent exchange flow in a vertical pipe

Arakeri and coworkers [3] performed experiments in which a flow in a vertical tube is driven by an unstable density difference across the tube. They placed a brine solution at the top and distilled water at the bottom. This system has significant similarities with RBC [3]. Note however that the above system does not have walls or boundary layers at the top and bottom; this feature helps us study the ultimate regime quite conveniently. Exchanging the top and bottom containers will lead to behaviour similar to stably-stratified flows.

2.8.4. Bubbly flow

Bubbles are introduced in a tank in which turbulence is generated by an active grid [88]. Naturally this system has certain similarities with RBC.

2.9. Non-Boussinesq flows

The Oberbeck–Boussinesq approximation provides a useful simplification for the analysis of fluid flows with small temperature difference between the two plates. For example, for water at normal temperature and pressure, the thermal expansion coefficient $\alpha \approx 2 \times 10^{-4}$. Therefore, for a temperature difference $\Delta \approx 30$ K, $(\delta\rho)/\rho \approx \alpha\Delta \approx 10^{-2}$, which is small, thus justifying the incompressible equation $\nabla \cdot \mathbf{u} = 0$. Also, the variation of ν and κ for temperature interval of ~ 10 K is quite negligible. Note however that in equation (25), the buoyancy term $\text{Ra Pr}\theta$ is comparable to the viscous term $\text{Pr}\nabla^2\mathbf{u}$. To illustrate, we estimate the ratio of the two terms near the onset of Rayleigh–Bénard instability for free-slip boundary condition as

$$\frac{\text{Ra Pr}\theta_{\text{rms}}}{\text{Pr}\nabla^2 u_{\text{rms}}} \approx \frac{\text{Ra}}{k^2} \frac{\theta_{\text{rms}}}{u_{\text{rms}}} \approx \frac{27\pi^4}{4k^2} \frac{1}{k^2} \approx 3. \quad (54)$$

Here $k = \sqrt{k_c^2 + \pi^2} = \sqrt{(\pi^2/2) + \pi^2}$ is the magnitude of the wavenumber associated with the convective role [23], and $u_{\text{rms}}/\theta_{\text{rms}} \approx k^2$ along the unstable eigenvector of the stability matrix. We expect the above trend to continue for large Ra as well, but this issue needs to be investigated in detail. These arguments show that the Oberbeck–Boussinesq approximation holds good for fluid like water at normal pressure and temperature for a temperature difference of order 10° .

Without Oberbeck–Boussinesq approximation, we would need to solve the equations for the velocity, density, and temperature fields. For further discussion, refer to Ahlers *et al* [1], Horn *et al* [46], and Sameen *et al* [92]. The above description, called *non-Boussinesq convection*, is useful in stellar convection where the temperature difference is too large for the Oberbeck–Boussinesq approximation to be valid. This topic, however, is beyond the scope of this paper.

In the next section, we will relate the turbulence behaviour of the above systems.

3. Spectra and fluxes of buoyancy-driven turbulence

3.1. Definitions

We can derive the time-evolution equation for $E_u(k)$ using equation (11) as [58, 112]

$$\frac{\partial E_u(k)}{\partial t} = T_u(k) + F_B(k) + F_{\text{ext}}(k) - D(k), \quad (55)$$

where $T_u(k)$ is the energy transfer rate to the shell k due to nonlinear interaction, and $F_B(k)$ and $F_{\text{ext}}(k)$ are the energy supply rates to the shell from the buoyancy and external forcing \mathbf{f}_u respectively, i.e.,

$$F_B(k) = - \sum_{|\mathbf{k}|=k} g \Re \langle u_z(\mathbf{k}) \rho^*(\mathbf{k}) \rangle, \quad (56)$$

$$F_{\text{ext}}(k) = \sum_{|\mathbf{k}|=k} \Re \langle \mathbf{u}(\mathbf{k}) \cdot \mathbf{f}_u^*(\mathbf{k}) \rangle. \quad (57)$$

For brevity we set $\rho_m = 1$. In equation (55), $D(k)$ is the viscous dissipation rate defined by

$$D(k) = \sum_{|\mathbf{k}|=k} 2\nu k^2 E_u(k). \quad (58)$$

The kinetic energy (KE) flux $\Pi_u(k_0)$, which is defined as the kinetic energy leaving a wavenumber sphere of radius k_0 due to nonlinear interactions, is related to the nonlinear interaction term $T_u(k)$ as

$$\Pi_u(k) = - \int_0^k T_u(k) dk. \quad (59)$$

Under a steady state ($\partial E_u(k)/\partial t = 0$), using equations (55) and (59), we deduce that

$$\frac{d}{dk} \Pi_u(k) = F_B(k) + F_{\text{ext}}(k) - D(k) \quad (60)$$

or

$$\Pi_u(k + \Delta k) = \Pi_u(k) + [F_B(k) + F_{\text{ext}}(k) - D(k)] \Delta k. \quad (61)$$

In computer simulations, the KE flux, $\Pi_u(k_0)$, is computed using the following formula [32, 111],

$$\Pi_u(k_0) = \sum_{k > k_0} \sum_{p \leq k_0} \delta_{\mathbf{k}, \mathbf{p}+\mathbf{q}} \mathcal{J}([\mathbf{k} \cdot \mathbf{u}(\mathbf{q})][\mathbf{u}^*(\mathbf{k}) \cdot \mathbf{u}(\mathbf{p})]). \quad (62)$$

Similarly, the potential energy (PE) flux $\Pi_\rho(k_0)$ is the potential energy leaving a wavenumber sphere of radius k_0 , which is computed using

$$\Pi_\rho(k_0) = \sum_{k > k_0} \sum_{p \leq k_0} \delta_{\mathbf{k}, \mathbf{p}+\mathbf{q}} \mathcal{J}([\mathbf{k} \cdot \mathbf{u}(\mathbf{q})][b^*(\mathbf{k})b(\mathbf{p})]), \quad (63)$$

where b is defined in equation (30). For RBC, we replace \mathbf{u} and b by nondimensional \mathbf{u} and θ respectively.

For a more detailed description of the energy transfers, we divide the wavenumber space into a set of wavenumber shells. The energy contents of a wavenumber shell of radius k and of unit width is denoted by $E(k)$. The shell-to-shell energy transfer rate from the velocity field of the m th shell to the velocity field of the n th shell is defined as

$$T_n^m = \sum_{\mathbf{k} \in n} \sum_{\mathbf{p} \in m} \delta_{\mathbf{k}, \mathbf{p}+\mathbf{q}} \mathcal{J}([\mathbf{k} \cdot \mathbf{u}(\mathbf{q})][\mathbf{u}^*(\mathbf{k}) \cdot \mathbf{u}(\mathbf{p})]). \quad (64)$$

One of the most interesting problems in the field of buoyancy driven turbulence is the scaling of energy spectrum and flux [63, 90]. In the next section, we will review some of the theoretical results obtained for the aforementioned topic.

3.2. Turbulence phenomenology

3.2.1. Classical Bolgiano-Obukhov scaling for SST

For the inertial range of isotropic hydrodynamic turbulence, Kolmogorov [50] first proposed a phenomenology according to which the energy spectrum in the inertial range is independent of the fluid properties and nature of large-scale forcing. He showed that the one-dimensional energy spectrum $E(k) = K_{\text{Ko}} \Pi_u^{2/3} k^{-5/3}$ in the inertial range of wavenumbers, where $\Pi_u(k)$ is the constant energy flux, and K_{Ko} is the Kolmogorov's constant.

Buoyancy (forcing) act at all scales, hence Kolmogorov's theory may not work for the buoyancy-driven turbulence. In this section we will describe how the buoyancy affects the energy spectra and fluxes of the buoyancy-driven flows. For stable stratification, Bolgiano [11] and Obukhov [81] argued that the KE flux $\Pi_u(k)$ is depleted at different length scales due to the conversion of KE to PE via buoyancy ($u_z \rho g$). Subsequently, $\Pi_u(k)$ decreases with k , and $E_u(k)$ is steeper than that predicted by Kolmogorov's theory; we refer to the above as *BO phenomenology or scaling*. According to this phenomenology, for $L_B \ll l \ll L$, buoyancy is important and the buoyancy term is balanced by the nonlinear term [$\rho g \approx (\mathbf{u} \cdot \nabla) \mathbf{u}$]. Here L_B is the Bolgiano scale [11] and L is the large length scale or the box size. The force balance at wavenumber $k = 1/l$ yields

$$\rho_k g \approx k u_k^2. \quad (65)$$

According to BO phenomenology, PE has a constant flux, i.e., $\Pi_\rho \approx k u_k \rho_k^2 \approx \epsilon_\rho$. Hence,

$$u_k \approx \epsilon_\rho^{1/5} g^{2/5} k^{-3/5}, \quad (66)$$

$$\rho_k \approx \epsilon_\rho^{2/5} g^{-1/5} k^{-1/5}. \quad (67)$$

Therefore, the KE spectrum $E_u(k) \approx u_k^2/k$, PE spectrum $E_\rho(k) \approx \rho_k^2/k$, and $\Pi_u(k) \approx u_k^3 k$ are

$$E_u(k) = c_1 \epsilon_\rho^{2/5} g^{4/5} k^{-11/5}, \quad (68)$$

$$E_\rho(k) = c_2 \epsilon_\rho^{4/5} g^{-2/5} k^{-7/5}, \quad (69)$$

$$\Pi_u(k) = c_3 \epsilon_\rho^{3/5} g^{6/5} k^{-4/5}, \quad (70)$$

$$\Pi_\rho(k) = \epsilon_\rho, \quad (71)$$

where c_i 's are constants. At smaller length scales ($k > k_B$), where $k_B = 2\pi/L_B$ is the Bolgiano wavenumber, Bolgiano [11] and Obukhov [81] argued that the buoyancy is relatively weak, hence Kolmogorov-Obukhov (KO) scaling is valid in this regime, i.e.,

$$E_u(k) = K_{Ko} \epsilon_u^{2/3} k^{-5/3}, \quad (72)$$

$$E_\rho(k) = K_{Ba} \epsilon_u^{-1/3} \epsilon_\rho k^{-5/3}, \quad (73)$$

$$\Pi_u(k) = \epsilon_u, \quad (74)$$

$$\Pi_\rho(k) = \epsilon_\rho, \quad (75)$$

where K_{Ba} is the Batchelor's constant. A comparison of $\Pi_u(k)$ of equation (70) with that of equation (74) yields the crossover wavenumber k_B as

$$k_B \approx g^{3/2} \epsilon_u^{-5/4} \epsilon_\rho^{3/4}. \quad (76)$$

The associated length, the Bolgiano length, is $L_B = (2\pi)/k_B$.

The scaling relations are also presented using the variables $\delta u_{||}(l)$ and $\delta\theta(l)$, which are defined as

$$\delta u_{||}(l) = [\mathbf{u}(\mathbf{x} + \mathbf{l}) - \mathbf{u}(\mathbf{x})] \cdot \frac{\mathbf{l}}{l}, \quad (77)$$

$$\delta\theta(l) = \theta(\mathbf{x} + \mathbf{l}) - \theta(\mathbf{x}), \quad (78)$$

and the structure function for the velocity and temperature fluctuations, which are defined as

$$S_q^u(l) = \langle [\delta u_{||}(l)]^q \rangle, \quad (79)$$

$$S_q^\theta(l) = \langle [\delta\theta(l)]^q \rangle, \quad (80)$$

where $\langle \cdot \rangle$ represent the ensemble average. Using scaling analysis similar to that given above, it can be derived that [29]

$$S_q^u(l) = \langle \epsilon_\rho \rangle^{q/5} g^{2q/5} l^{3q/5}, \quad (81)$$

$$S_q^\theta(l) = \langle \epsilon_\rho \rangle^{2q/5} g^{-q/5} l^{q/5} \quad (82)$$

for $l > L_B$, and

$$S_q^u(l) = \langle \epsilon_u \rangle^{q/3} l^{q/3}, \quad (83)$$

$$S_q^\theta(l) = \langle \epsilon_u \rangle^{-q/6} \langle \epsilon_\rho \rangle^{q/2} l^{q/3} \quad (84)$$

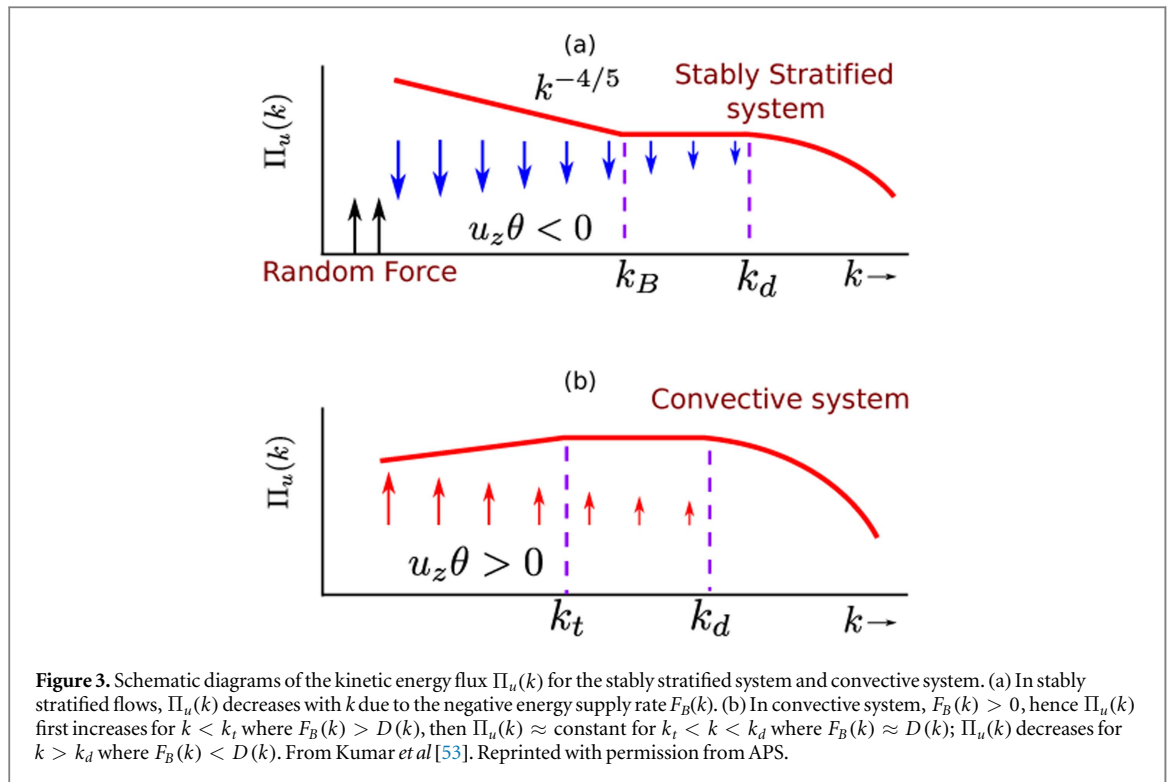
for $l < L_B$. Note that l correspond to $1/k$, and $\delta u_{||}(l) \rightarrow u_k$.

The BO phenomenology implicitly assumes isotropy in Fourier space, which is a tricky assumption. For BO scaling, the gravity must be strong enough to compete with the nonlinear term $\mathbf{u} \cdot \nabla \mathbf{u}$, but not too strong to make the flow quasi two-dimensional (quasi-2D). This corresponds to $Fr \approx 1$ regime. A large number of earlier explorations in SST have been for $Fr \ll 1$ regime, see for example, Lindborg [60], Brethouwer *et al* [14], and Bartello and Tobias [4]. SST can be broadly classified in three regimes. Note that nonlinearity is strong ($Re \gg 1$) for turbulent flows.

- (i) Weak gravity ($Ri \ll 1$): Strong nonlinearity yields behaviour similar to hydrodynamic turbulence ($E_u(k) \sim k^{-5/3}$).
- (ii) Moderate gravity ($Ri \approx 1$): Comparable strengths of gravity and nonlinearity yields nearly isotropic turbulence with BO scaling, as described earlier.
- (iii) Strong gravity ($Ri \gg 1$): Strong gravity makes the flow quasi-2D. Hence the behaviour has similarities with 2D hydrodynamic turbulence (e.g., inverse cascade of energy). Refer to Lindborg [60], Brethouwer *et al* [14], and Bartello and Tobias [4] for further details.

3.2.2. Generalization of Bolgiano-Obukhov scaling to RBC

Using mean field theory approximation, Procaccia and Zeitak [89] argued that the Bolgiano-Obukhov scaling is applicable to convective turbulence. Later, L'vov [65] assumed that in convective turbulence, the kinetic energy is converted to the potential energy and therefore, favored BO scaling. L'vov and Falkovich [66] employed a differential model for energy and entropy fluxes in k -space and found that the BO scaling is valid for convective turbulence. Rubinstein [91] employed renormalization group analysis to RBC and observed that the



renormalized viscosity $\nu(k) \sim k^{-8/5}$, $E_u(k) \sim k^{-11/5}$, and $E_p(k) \sim k^{-7/5}$. Based on these observations Rubinstein claimed BO scaling for RBC. Ching [27, 29] and Ching *et al* [28] studied the structure functions for the velocity and temperature fluctuations of turbulent convection, and claimed consistency with Bolgiano-Obukhov scaling. Ching *et al* [28] computed the anomalous scaling for the turbulent RBC.

The aforementioned theories had a profound influence in the field, and a large number of analytical, experimental, and numerical works have been attempted to verify these ideas. Lohse and Xia [63] reviewed critically if BO scaling is indeed present in RBC; they studied the experimental, theoretical, and numerical results and argued that it is difficult to conclude the applicability of BO scaling in RBC. Recently Kumar *et al* [53] showed that the BO scaling does not describe RBC turbulence since the energy supply by buoyancy in RBC is very different from that in stably stratified flow. We will provide these arguments below.

3.2.3. A phenomenological argument based on kinetic energy flux

Kumar *et al* [53] and Verma *et al* [114, 115] presented a phenomenological argument based on the KE flux to derive a spectral theory of buoyancy-driven turbulence. Equation (61) provides important clues on the energy spectrum and flux of the buoyancy-driven flows. Here we list three possibilities for the inertial range ($k_f < k < k_d$), where k_f is the forcing wavenumber, and k_d is the dissipation wavenumber:

- (i) For the inertial range of hydrodynamic turbulence, $F_B(k) = 0$ and $D(k) \rightarrow 0$, therefore $\Pi_u(k + \Delta k) \approx \Pi_u(k)$ and $E_u(k) \sim k^{-5/3}$, which is a prediction of the Kolmogorov's theory [50]. Note that $F_{\text{ext}}(k) = 0$ in the inertial range.
- (ii) For the stably stratified flows, as argued by Bolgiano [11] and Obukhov [81], in the $k_f < k < k_B$ wavenumber band, buoyancy converts the kinetic energy of the flow to the potential energy, i.e., $F_B(k) < 0$. Hence, equation (61) predicts that $\Pi_u(k)$ will decrease with k in this wavenumber range, as shown in figure 3(a). In the wavenumber range, $k_B < k < k_d$, buoyancy becomes weaker, hence $\Pi_u(k) \approx \text{constant}$.
- (iii) For RBC in three dimensions, buoyancy feeds the kinetic energy, hence $F_B(k) > 0$. Therefore we expect the KE flux $\Pi_u(k)$ to increase. Numerical simulation of Kumar *et al* [53] for $\text{Pr} = 1$ and large Ra show that the energy supplied by buoyancy is dissipated by the viscous force, i.e., $F_B(k) \approx D(k)$. Hence $\Pi_u(k) \approx \text{constant}$ in the inertial range, and they recovered Kolmogorov's spectrum for RBC for $\text{Pr} = 1$ in 3D. Note that L'vov [65] argued that $F_B(k) < 0$, which is not the case in 3D RBC with $\text{Pr} \approx 1$. Note that the nature of energy flux depends on the space dimensionality and Prandtl number, some of which will be discussed in subsequent section.

The above arguments indicate that the structure functions for the fluctuations of RBC in 3D for $\text{Pr} \approx 1$ may follow the following scaling relations:

$$S_q^u(l) = \langle \epsilon_u \rangle^{q/3} l^{q/3}, \quad (85)$$

$$S_q^\theta(l) = \langle \epsilon_u \rangle^{-q/6} \langle \epsilon_\rho \rangle^{q/2} l^{q/3}. \quad (86)$$

The above relations need to be tested using numerical simulation and experiments.

3.2.4. Modeling and field theory

Researchers [33, 51, 59, 68, 69, 121] employed field-theoretic techniques to understand the physics of turbulent fluid. In field theory, the nonlinear terms of the equations are expanded perturbatively. Some of the popular field-theoretic techniques are direct interaction approximation (DIA) [51, 59], renormalization group analysis [33, 51, 68, 69, 121], mean field approximation [89], etc. Field theory has been applied to buoyancy-driven flows as well.

As described in section 3.2.2, Procaccia and Zeitak [89] employed mean field approximation to convective turbulence and obtained BO scaling. Rubinstein [91] used Yaghot-Orszag's [121] renormalization group procedure and proposed an isotropic model for convective turbulence. His results are consistent with that of Procaccia and Zeitak [89]. Recently, using self-consistent field theory, Bhattacharjee [7] obtained $E_u(k) \sim k^{-13/3}$ for RBC in the infinite Prandtl number limit. Bhattacharjee [6] used the global energy balance for the stratified fluid and argued that the BO scaling could be observed in stably stratified flow at high Richardson number. In addition, he also added the possibility of BO scaling for RBC in some range of Prandtl numbers.

In the next section, we will present numerical results for the stably stratified turbulence and RBC.

3.3. Numerical analysis of buoyancy-driven turbulence

3.3.1. Stably stratified turbulence

Researchers simulated the SST for the three regimes described in section 3.2.1. First we discuss the results for strong gravity that corresponds to $\text{Ri} \gg 1$ or $\text{Fr} \ll 1$. Such configurations are observed in some regimes of planetary and stellar atmospheres. Strong gravity makes such flows quasi-2D with dual scaling, k^{-3} and $k^{-5/3}$. In this regime, Lindborg [60], Brethouwer *et al* [14], and Bartello and Tobias [4] showed that the spectra of the horizontal KE and PE follow $k_\perp^{-5/3}$ scaling, while the energy spectrum of the vertical velocity follows k_\parallel^{-3} . Vallgren *et al* [109] included rotation in their simulation and obtained KE spectrum as k^{-3} and $k^{-5/3}$ for two different wavenumber bands.

For weak stratification ($\text{Ri} \ll 1$), Kumar *et al* [53] performed a 3D SST simulation and reported Kolmogorov's spectrum for the kinetic energy as expected. Kumar *et al* also studied the moderate stratification regime and reported BO scaling, which will be described below. In this paper we focus on the results for $\text{Fr} \approx 1$ since they have been observed recently.

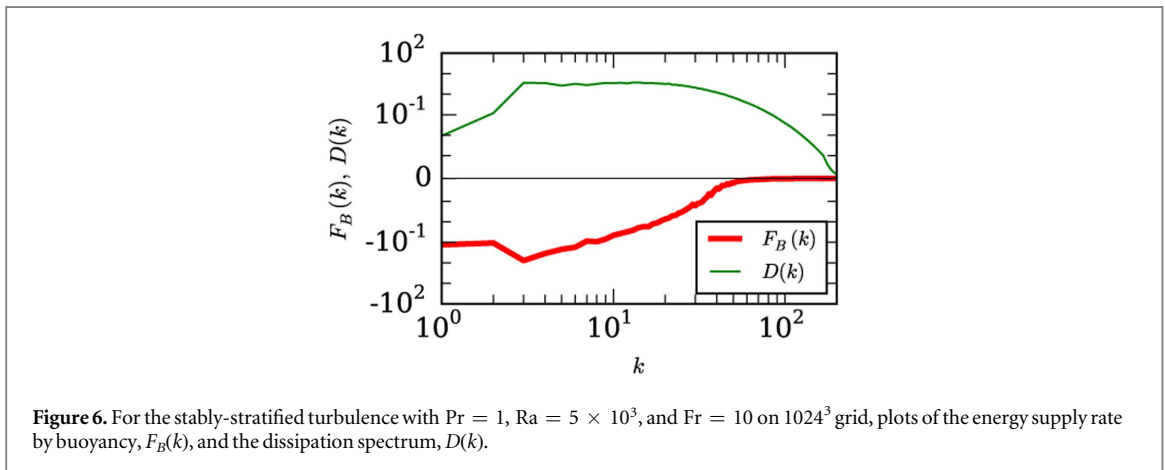
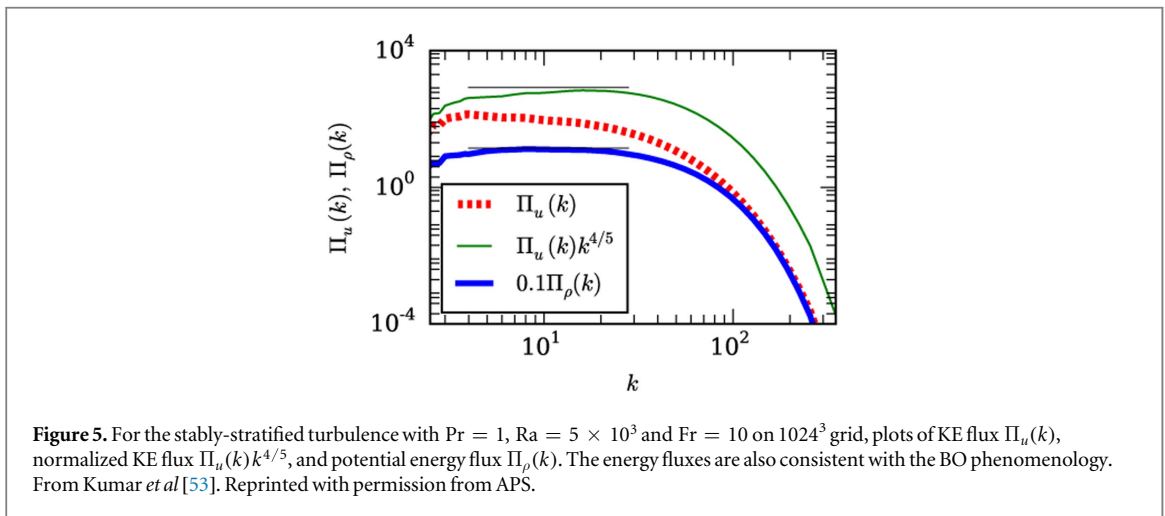
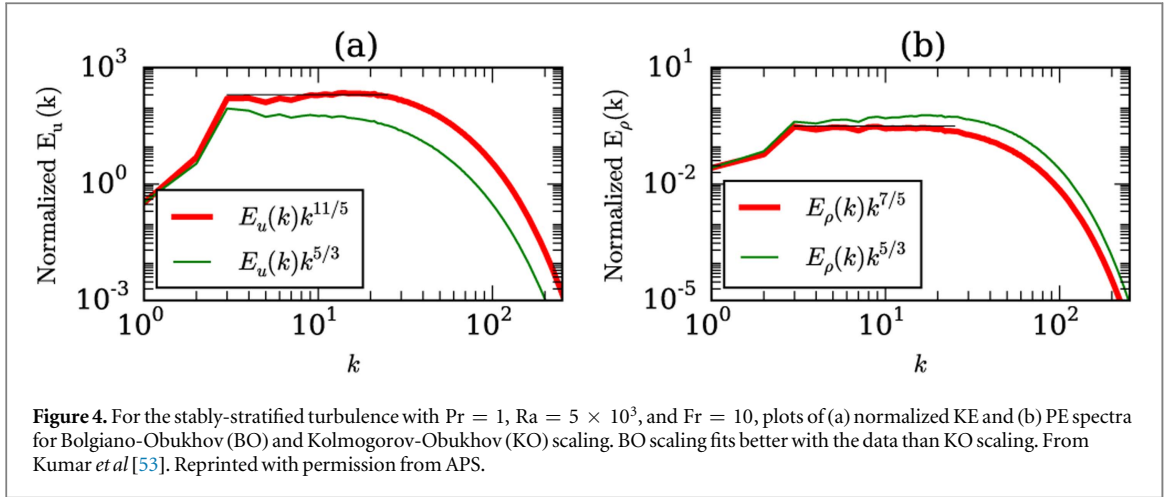
Kumar *et al* [53] simulated stably stratified flows in a cubical box of size $(2\pi)^3$ with periodic boundary conditions at all the walls. They forced the small wavenumber modes randomly to achieve a steady state. The parameters of their simulations are $\text{Ra} = 5 \times 10^3$ and $\text{Pr} = 1$ that yields $\text{Ri} = 0.01$ and $\text{Fr} = 10$. Figure 4(a) exhibits the normalized KE spectra— $E_u(k)k^{11/5}$ for the BO scaling, and $E_u(k)k^{5/3}$ for the KO scaling. The numerical data fits better with the BO scaling than the KO scaling, thus confirming the BO phenomenology for the SST when $\text{Fr} \approx 1$. This is also verified by the PE spectrum as shown in figure 4(b) in which $E_\rho(k)k^{7/5}$ provides a better fit to the data than $E_\rho(k)k^{5/3}$.

Further, Kumar *et al* [53] computed the KE and PE fluxes which are exhibited in figure 5. They observed that $\Pi_u(k) > 0$ and it decreases with k (equation (70)), while the PE flux Π_ρ is a constant in the inertial range (equation (71)); thus the flux results are consistent with the BO predictions. Kumar *et al* [53] also computed the energy supply rate by buoyancy, $F_B(k)$, and the viscous dissipation spectrum, $D(k)$, which are illustrated in figure 6. Note that $F_B(k) < 0$, as argued in BO phenomenology. The Bolgiano wavenumber k_B of equation (76) is approximately 8.5, which is only 3–4 times smaller than k_δ , the wavenumber where the dissipation range starts. Therefore Kumar *et al* [53] did not observe a definitive crossover from $k^{-11/5}$ to $k^{-5/3}$ in their simulations.

The aforementioned observations demonstrate applicability of the BO scaling for SST with a moderate stratification.

3.3.2. Rayleigh–Bénard convection

A large number of numerical simulations have been performed with an aim to identify which among the two, BO or KO, scaling is applicable to RBC [63]. Grossmann and Lohse [37] simulated RBC for $\text{Pr} = 1$ under Fourier–Weierstrass approximation and reported Kolmogorov's scaling. For on periodic boundary condition,



Borue and Orszag [12] and Škandera *et al* [100] reported KO scaling for the velocity and temperature fields. Kerr [49] reported the horizontal spectrum as a function of horizontal wavenumber and observed Kolmogorov's spectrum. Verzicco and Camussi [117], and Camussi and Verzicco [20] showed BO scaling using the frequency spectrum of real space probe data. Kaczorowski and Xia [48] reported KO scaling for the longitudinal velocity structure functions, but BO scaling for the temperature structure functions in the centre of a cubical cell. Kumar *et al* [53] computed $E_u(k)$ and $\Pi_u(k)$, and showed Kolmogorov-like behaviour for RBC, i.e., $E_u(k) \sim k^{-5/3}$ and $\Pi_u(k) \sim \text{const}$. In this paper we present the above quantities for 4096^3 resolution and very high Ra that unambiguously demonstrates KO scaling for RBC. We also report the shell-to-shell energy transfers and the ring spectrum for RBC that show close resemblance with the hydrodynamic turbulence.

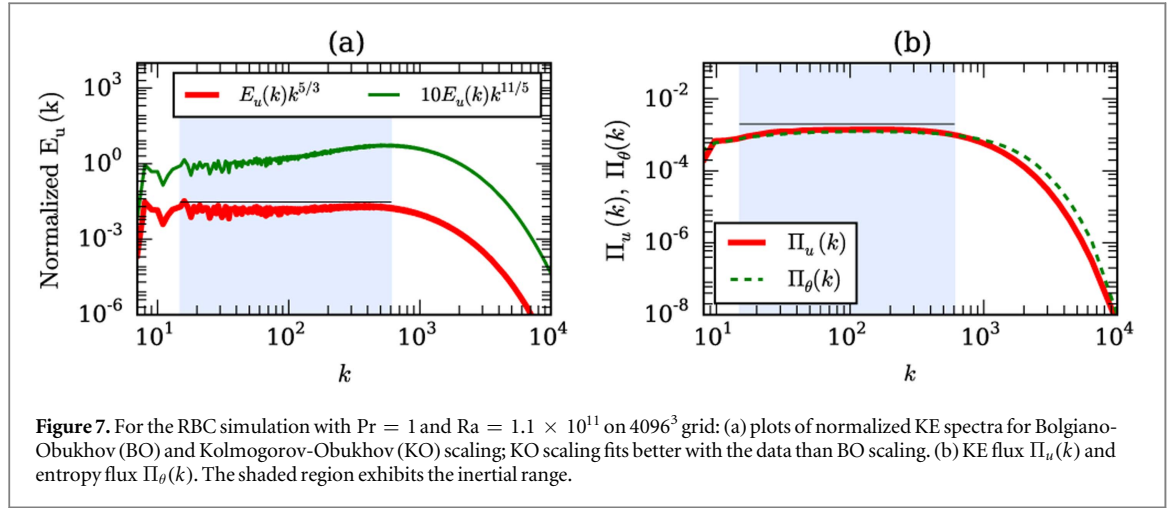


Figure 7. For the RBC simulation with $Pr = 1$ and $Ra = 1.1 \times 10^{11}$ on 4096^3 grid: (a) plots of normalized KE spectra for Bolgiano-Obukhov (BO) and Kolmogorov-Obukhov (KO) scaling; KO scaling fits better with the data than BO scaling. (b) KE flux $\Pi_u(k)$ and entropy flux $\Pi_\theta(k)$. The shaded region exhibits the inertial range.

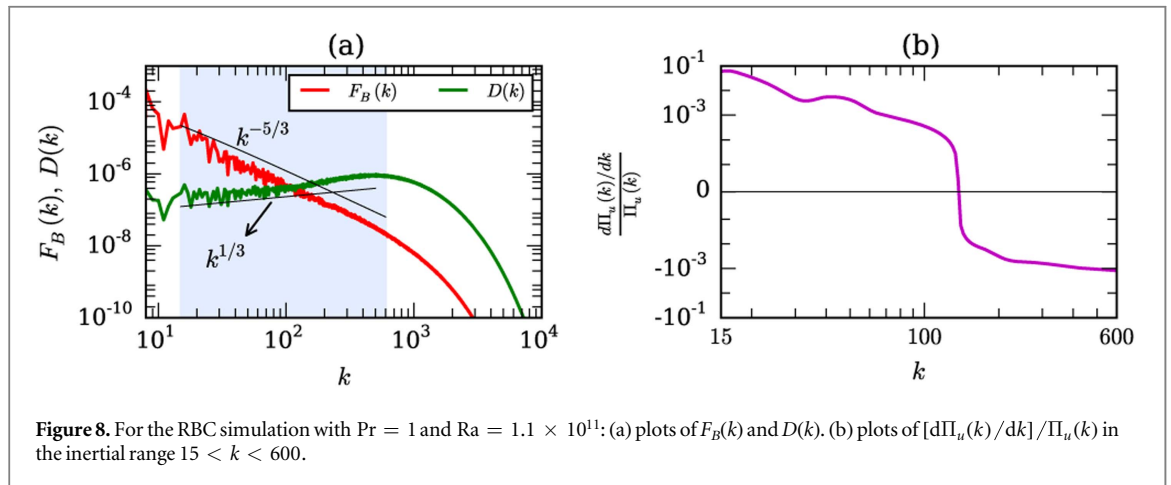


Figure 8. For the RBC simulation with $Pr = 1$ and $Ra = 1.1 \times 10^{11}$: (a) plots of $F_B(k)$ and $D(k)$. (b) plots of $[d\Pi_u(k)/dk]/\Pi_u(k)$ in the inertial range $15 < k < 600$.

We performed RBC simulations in a unit box with 4096^3 grid for $Pr = 1$ and $Ra = 1.1 \times 10^{11}$. For the velocity field, we employed the free-slip boundary condition at the top and bottom plates, and periodic boundary condition at the side walls. The temperature field satisfies conducting boundary condition at the top and bottom plates, and the periodic boundary condition at the side walls. We computed the spectra and fluxes of the KE and the entropy ($\theta^2/2$) using the steady state data. Figure 7(a) exhibits the KE spectra normalized with $k^{11/5}$ and $k^{5/3}$. The plots indicate that in the wavenumber band $15 < k < 600$ (inertial range), the shaded region of the figure, the KO scaling fits better than the BO scaling.

We exhibit the KE and entropy fluxes in figure 7(b). We observe that the kinetic energy flux $\Pi_u(k)$ remains constant in the inertial range, a band where $E_u(k) \sim k^{-5/3}$. Thus we claim that the convective turbulence exhibits Kolmogorov's power law in the inertial range. We also computed $F_B(k)$, $\Pi_u(k)$, and $d\Pi_u(k)/dk$ as further tests. According to figure 8(a) $F_B(k) > 0$ in the inertial range, consistent with the discussion of section 3.2.3 and figure 3(b), and it approximately balances $D(k)$. Therefore, $d\Pi_u(k)/dk \approx 0$ or $\Pi_u(k) \approx \text{constant}$ (see equation (60)). The constancy of $\Pi_u(k)$ yields $E_u(k) \sim k^{-5/3}$, consistent with the energy spectrum plots of figure 7(a). Figure 8(b) shows that $[d\Pi_u(k)/dk]/\Pi_u(k) \ll 1$ in the inertial range consistent with the constant $\Pi_u(k)$. Interestingly, $D(k) = 2\nu k^2 E_u(k) \sim k^{1/3}$, consistent with $E_u(k) \sim k^{-5/3}$. Also, $F_B(k) \sim k^{-5/3}$. In addition, the entropy flux $\Pi_\theta(k)$ is constant, and $\Pi_u(k) \approx \Pi_\theta(k)$ in dimensionless units.

We also compute the shell-to-shell energy transfers (equation (64)) using the steady-state data of our simulation. We divide the Fourier space into 40 concentric shells; the inner and outer radii of the n th shell are k_{n-1} and k_n respectively with $k_n = \{0, 2, 4, 8, 8 \times 2^{s(n-3)}, \dots, 6432\}$, where $s = (1/35) \log_2(804)$. The radii of the inertial-range shells are binned logarithmically due to the power law physics of RBC in the inertial range. In figure 9(a) we exhibit the shell-to-shell energy transfers with the indices of the x , y axes representing the receiver and giver shells respectively. The plot indicates that m th shell gives energy to $(m + 1)$ th shell, and it receives energy from the $(m - 1)$ th shell [111]. Thus the energy transfer in RBC is local and forward, very similar to hydrodynamic turbulence. This result is consistent with the energy spectrum and flux studies described earlier.

Convective flows are expected to be anisotropic due to buoyancy; hence it is important to quantify anisotropy using the quantities that are dependent on the polar angle, the angle between \hat{z} and \mathbf{k} . For the same,

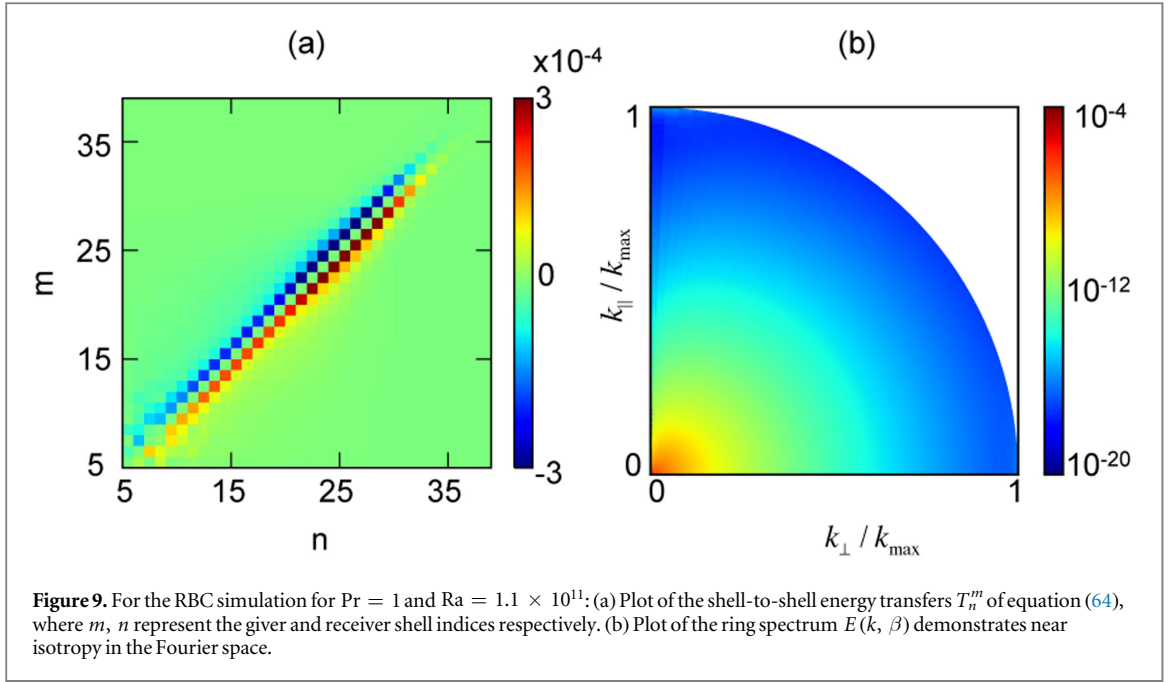


Figure 9. For the RBC simulation for $Pr = 1$ and $Ra = 1.1 \times 10^{11}$: (a) Plot of the shell-to-shell energy transfers T_n^m of equation (64), where m, n represent the giver and receiver shell indices respectively. (b) Plot of the ring spectrum $E(k, \beta)$ demonstrates near isotropy in the Fourier space.

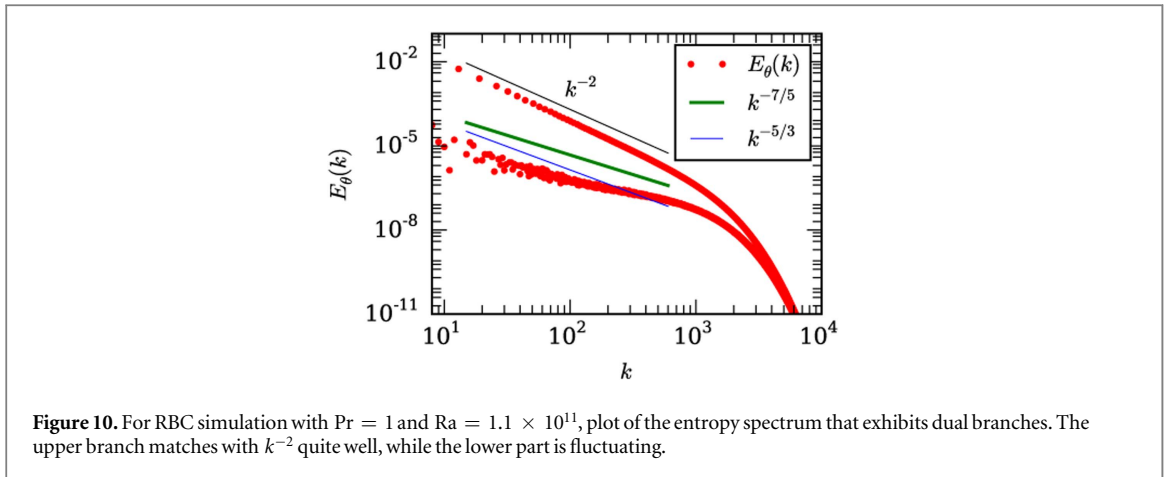


Figure 10. For RBC simulation with $Pr = 1$ and $Ra = 1.1 \times 10^{11}$, plot of the entropy spectrum that exhibits dual branches. The upper branch matches with k^{-2} quite well, while the lower part is fluctuating.

we divide a wavenumber shell into rings [75]. The energy contents of the rings are called *ring spectrum* $E(k, \beta)$, where β represents the sector index for the polar angles (for details see Nath *et al* [75]). The ring spectrum $E(k, \beta)$, depicted in figure 9(b), shows that the flow is nearly isotropic, again similar to hydrodynamic turbulence. These results clearly demonstrate that the turbulent convection for $Pr = 1$ has a very similar behavior as hydrodynamic turbulence.

The temperature fluctuation however exhibit a unique behaviour. As illustrated in figure 10, we observe dual branches for the entropy spectrum ($E_{\theta}(k)$). The upper branch varies as k^{-2} because $\theta(0, 0, k_z) \approx -1/(\pi k)$, as discussed in section 2.7. The lower branch shows neither KO ($k^{-5/3}$) nor BO ($k^{-7/5}$) spectrum. Note that both the branches of entropy spectrum generate a constant entropy flux $\Pi_{\theta}(k)$ (see figure 7(b)), and the modes $\theta(0, 0, k_z)$ also participate in energy transfers.

3.4. Experimental results

For stably-stratified flows, there are not many laboratory experiments to verify BO phenomenology. However, scientists have measured the KE spectrum of the Earth's atmosphere and relate it to the theoretical predictions. Most notably Gage and Nastrom [35] observed a combination of k^{-3} and $k^{-5/3}$ energy spectra. Some researchers attribute the k^{-3} spectrum at lower wavenumbers to the two-dimensionalization of the flow, while $k^{-5/3}$ spectrum at larger wavenumbers to the forward cascade of kinetic energy; yet these issues are still unresolved. These features are expected to arise for $Fr \ll 1$.

There are a significant number of laboratory experiments on RBC, with some favouring the BO scaling [25, 124], while some others in support of the KO scaling [30]. These results are reviewed in detail in Lohse and Xia [63]. In most convective experiments, the velocity field, $u_z(\mathbf{r}, t)$, and/or the temperature field, $T(\mathbf{r}, t)$, are

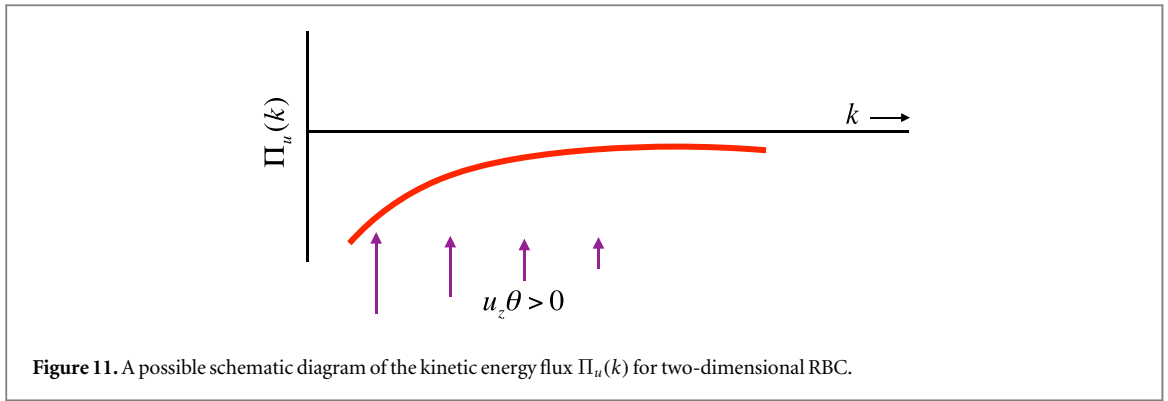


Figure 11. A possible schematic diagram of the kinetic energy flux $\Pi_u(k)$ for two-dimensional RBC.

probed near the lateral walls of the container. For such experiments, the Taylor's hypothesis [56, 94, 105] is invoked to relate the frequency power spectrum $E(f)$ of the time series to the one-dimensional wavenumber spectrum $E(k)$; this connection is under debate due to the absence of any constant mean velocity field [56, 63]. Researchers [57, 104, 122, 123] employ 2D particle image velocimetry for high-resolution visualization and computation of an approximate energy spectrum under the assumption of homogeneity and isotropy, which is not strictly valid in convection [75]. In summary, on the experimental front, there is no convergence on which of the two scaling, BO of KO, is valid. For details refer to the review papers [2, 63].

3.5. Turbulence in thermal boundary layer and in two dimensions

A burning question is whether KO scaling or BO scaling is applicable to the boundary layers of RBC. The flux arguments of section 3.2.3 provide some insights into the dynamics of boundary layers. Here, typically $u_z \ll u_\perp$, hence the flow is quasi-2D, and we expect an inverse cascade of KE. Using $\Pi_u(k) < 0$, $F_B(k) > 0$, and $d\Pi_u(k)/dk \approx F_B(k)$, we may argue that $\Pi_u(k)$ may increase with k as shown in figure 11. An application of scaling arguments of section 3.2.1 may yield $E_u(k)$ and $|\Pi_u(k)|$ according to equations (68)–(71), i.e., Bolgiano–Obukhov scaling for $k < k_B$. For $k > k_B$, the KE spectrum may exhibit a mixture of $k^{-5/3}$ (regime of inverse cascade of energy) and k^{-3} (regime of forward cascade of enstrophy) depending on where the effective forcing band lies in relation to k_B . Thus, in the boundary layer, RBC may exhibit BO scaling, and it needs to be investigated carefully using numerical simulations and experiments.

The aforementioned scaling arguments may also work for 2D RBC (xz plane in which the buoyancy is along the z direction), as well as in quasi 2D RBC (when $L_x \gg L_y$). Toh and Suzuki [106] simulated 2D RBC and reported $E_u(k) \sim k^{-11/5}$ and $\Pi_u(k) \sim -k^{-4/5}$ in line with the above arguments. Calzavarini *et al* [19] also reported similar results in their structure function computations.

3.6. Turbulence in RTI

RTI has a strong similarity with RBC in the sense that the heavier fluid sits on top of lighter fluid. Hence we expect the RBC turbulence phenomenology to be applicable to RTI as well, at least approximately. Chertkov [24] proposed that a fully-developed 3D RTI will exhibit Kolmogorov's spectrum due to the Rayleigh–Taylor pumping at large scales. Boffetta *et al* [10] observed this behaviour in their numerical simulations. Chertkov [24] however does not take into account the buoyancy at all scales (see section 3.2.3). In a quasi-2D box ($L_y \ll L_x$), Boffetta *et al* [9] show coexistence of BO and KO scaling ($k^{-11/5}$ and $k^{-5/3}$), consistent with the arguments of section 3.5.

3.7. Turbulence in miscellaneous systems

Scientists have studied spectra of the velocity field and the scalar field in other buoyancy-driven systems. Pawar and Arakeri [87] performed experiment on the vertical tube described in section 2.8.3. They observed that the velocity field exhibits $k^{-5/3}$ spectrum, while the scalar spectrum is closer to $k^{-7/5}$.

Prakash *et al* [88] studied the energy spectrum of the bubbly turbulence using an experiment. For the velocity field, they reported $k^{-5/3}$ energy spectrum for $k < 1/b$, and k^{-3} for $k > 1/b$ where b is the bubble size. They argued that the large and intermediate scales exhibit $k^{-5/3}$ spectrum due to the standard Kolmogorov's argument. For $k > 1/b$, Prakash *et al* [88] explained the k^{-3} energy spectrum by invoking equipartition between the energy dissipation and energy feed by the buoyancy. We believe that the Kolmogorov's spectrum for bubbly turbulence arises due to the dynamical similarities with RBC. For this system it may be interesting to investigate the energy spectrum using the flux arguments.

The turbulent Taylor–Couette flow [43] may exhibit spectral behaviour similar to RBC since both the systems are unstable with similar energetics (see sections 3.2.3 and 3.3.2). We believe that the Non-Boussinesq

convective flows may also exhibit Kolmogorov-like spectrum for weak compressibility since here too the thermal plumes feed the kinetic energy, as in RBC.

3.8. Turbulence in small and large Prandtl number RBC

In section 3.2.3 we derived the spectra and fluxes of the velocity and temperature fields for RBC with $Pr \sim 1$. These arguments are not applicable to RBC at extreme Prandtl numbers. However, we can easily deduce the spectrum for very small and very large Pr 's as follows. These computations have been first reported in [72] and [86] respectively.

In RBC with zero or small Prandtl numbers, thermal diffusivity $\kappa \rightarrow \infty$ that leads to $u_z(\mathbf{k}) \sim \theta(\mathbf{k})(\kappa k^2)$ [72]. Hence, the buoyancy, which is proportional to $\theta(\mathbf{k})$, is dominant at small wavenumbers. Therefore, the assumption of the Kolmogorov's phenomenology that the forcing acts at large length scales is valid, and we expect the Kolmogorov's phenomenology for the hydrodynamic turbulence to be applicable to RBC with $Pr \rightarrow 0$. Mishra and Verma [72] verified the above phenomenology using numerical simulations.

In the limit of infinite Prandtl number ($\nu \rightarrow \infty$), the momentum equation is linear [86]. However if the Péclet number is large, the temperature equation is nonlinear and it yields an approximate constant entropy flux. Using scaling arguments, Pandey *et al* [86] derived that for infinite and large Pr , $E_u(k) \sim k^{-13/3}$. They also verified the above scaling using numerical simulations.

3.9. Simulation of turbulent convection in a periodic box and shell model

Borue and Orszag [12], Škandera *et al* [100], Lohse and Toschi [62], and Calzavarani *et al* [18] simulated turbulent thermal convection in a periodic box. They simulated equations (17), (18) under a gradient $d\bar{T}/dz$. In the absence of boundary layers, the velocity and temperature fields exhibit $k^{-5/3}$ spectra [12, 100]. In addition, the Nusselt number $Nu \sim Ra^{1/2}$ [18, 62], which is expected in the ultimate regime when the effects of boundary layers are negligible. Note that the temperature spectrum for the periodic box is very different from that with conducting walls that exhibit dual spectra. It is important to note that turbulent thermal convection in a periodic box is numerically unstable; the system exhibits steady behaviour for carefully chosen set of initial conditions.

Direct numerical simulation of turbulent systems is quite demanding due a large number of interacting Fourier modes. Therefore, scientists often use shell models, which are based on much fewer number of modes. Brandenburg [13], Lozhkin and Frick [64], Mingshun and Shida [70], Ching and Cheng [28], and Kumar and Verma [54, 55] constructed shell models for buoyancy-driven turbulence. Ching [27, 29] and Ching *et al* [28] computed the structure functions of turbulent convection using a shell model, and claimed consistency with Bolgiano-Obukhov scaling. The advantage of the shell model of Kumar and Verma [54] is that it describes both turbulent stably-stratified and convective flows using a single set of equations. It also enables flux computation of the kinetic energy and $\rho^2/2$, where ρ is the density of the fluid. Kumar and Verma [54] showed that the results of the shell model are consistent with the DNS results described earlier.

3.10. Concluding remarks on the energy spectrum

We summarise the important results of this section as follows:

- (i) A large body of works on RBC assume Bolgiano-Obukhov scaling. The flux-based arguments described in sections 3.2.3 and 3.3.2 demonstrate that in three dimensions for Pr near unity, RBC exhibits Kolmogorov-like energy spectrum and flux. For example, the KE flux is nearly constant in the inertial range; the shell-to-shell energy transfer is local and forward; the ring spectrum exhibits a near isotropy in Fourier space. The constant KE flux is due to the near cancellation between the KE supply by buoyancy and the viscous dissipation rate.
- (ii) The nature of energy spectrum and flux of RBC depends on the space dimensionality and Prandtl number, as described earlier in this section. For small Prandtl number, convective turbulence is similar to hydrodynamic turbulence, but $E_u(k) \sim k^{-13/3}$ for very large and infinite Prandtl number.
- (iii) The small-scale fluctuations in the boundary layer contributes to $E_u(k)$ at large k . Hence the aforementioned $E_u(k)$ in the inertial range is dominated by the fluctuations of the bulk.
- (iv) The temperature fluctuations for RBC exhibits dual spectra, with the upper branch scaling as k^{-2} . In section 2.7 we discussed the origin of k^{-2} spectrum in terms of temperature profile in the boundary layers and in the bulk.
- (v) The SST under nearly isotropic conditions (when Froude number is of the order of unity) exhibits Bolgiano-Obukhov scaling.

In the next section, we briefly describe scaling of Reynolds and Nusselt numbers.

4. Modelling of large-scale quantities of RBC

In this section we quantify the large-scale quantities of RBC, namely the Nusselt and Reynolds numbers. Many researchers have worked on this problem; for details and references, refer to the review articles [2, 8, 26, 63, 98]. Despite complexities of the flow, RBC exhibits certain universal behaviour; in the turbulent limit, $Pe \sim \sqrt{Ra Pr}$, but in the viscous regime, $Pe \sim Ra^{3/5}$ [38, 84].

Turbulent thermal flux is somewhat more complex; it is quantified using the nondimensional variable called Nusselt number, Nu , which is defined as [2, 26, 119]

$$Nu = \frac{\kappa \Delta / d + \langle u_z \theta_{res} \rangle_V}{\kappa \Delta / d} = 1 + \left\langle \frac{u_z d}{\kappa} \frac{\theta_{res}}{\Delta} \right\rangle_V = 1 + C_{u\theta_{res}} \langle u_z'^2 \rangle_V^{1/2} \langle \theta_{res}'^2 \rangle_V^{1/2}, \quad (87)$$

where $\langle \rangle_V$ stands for a volume average, $u_z' = u_z d / \kappa$, $\theta_{res}' = \theta_{res} / \Delta$, and $C_{u\theta_{res}}$ is the normalized correlation function between the vertical velocity and the residual temperature fluctuation [116]:

$$C_{u\theta_{res}} = \frac{\langle u_z' \theta_{res}' \rangle_V}{\langle u_z'^2 \rangle_V^{1/2} \langle \theta_{res}'^2 \rangle_V^{1/2}}. \quad (88)$$

Kraichnan [52] argued that in turbulent convection $u_z' \sim Ra^{1/2}$, $\theta_{res}' \sim 1$, and $C_{u\theta_{res}} \sim \text{const}$, hence $Nu \sim Ra^{1/2}$, which is called the scaling of *ultimate regime*. Experiments and numerical simulations however reveal that $Nu \sim Ra^\beta$ with β ranging from 0.25 to 0.33. Grossmann and Lohse [38–42] derived a phenomenological formula that fits with the experimental and numerical results quite well. The deviation from Kraichnan's predictions of $1/2$ to ≈ 0.3 is attributed to the boundary layer [38, 39]. There are intense research activities to test whether the ultimate regime exists or not. He *et al* [44] and others performed experiments on turbulent convection up to $Ra \approx 10^{15}$ and observed an increase in the Nusselt-number exponent β from 0.31 to 0.38, as well as logarithmic mean temperature profile [108]. Thus they claimed existence of the ultimate regime. However, Niemela *et al* [79] and Urban *et al* [107] do not observe deviation of β from ≈ 0.3 , hence they argue against the existence of ultimate regime. In this paper, we do not discuss this issue any further, and we refer the reader to works described above.

In the next subsection we describe the Grossmann–Lohse model that predicts the scaling of Reynolds and Nusselt number quite successfully.

4.1. Grossmann–Lohse model

Grossmann and Lohse (GL) [38–42, 102] derived the formulas for $Nu(Ra, Pr)$ and $Re(Ra, Pr)$ by exploiting the fact that the global viscous dissipation rate, ϵ_u , and thermal dissipation rate, ϵ_T , get contributions from the bulk and boundary layers, i.e.,

$$\epsilon_u = \epsilon_{u,BL} + \epsilon_{u,bulk}, \quad (89)$$

$$\epsilon_T = \epsilon_{T,BL} + \epsilon_{T,bulk}, \quad (90)$$

where BL and bulk denote the boundary layer and the bulk respectively. They invoked the exact relations of Shraiman and Siggia [97] for the global viscous and thermal dissipation rates (see equations (38), (39)), and estimated the aforementioned contributions of the boundary layers and the bulk to ϵ_u and ϵ_T in various Ra – Pr regimes. For $Pr \approx 1$ and very large Ra they used $\epsilon_{u,bulk} = U^3/d$ and $\epsilon_{T,bulk} = U\Delta^2/d$, but for extreme Prandtl numbers, these estimates get altered by the boundary layer widths.

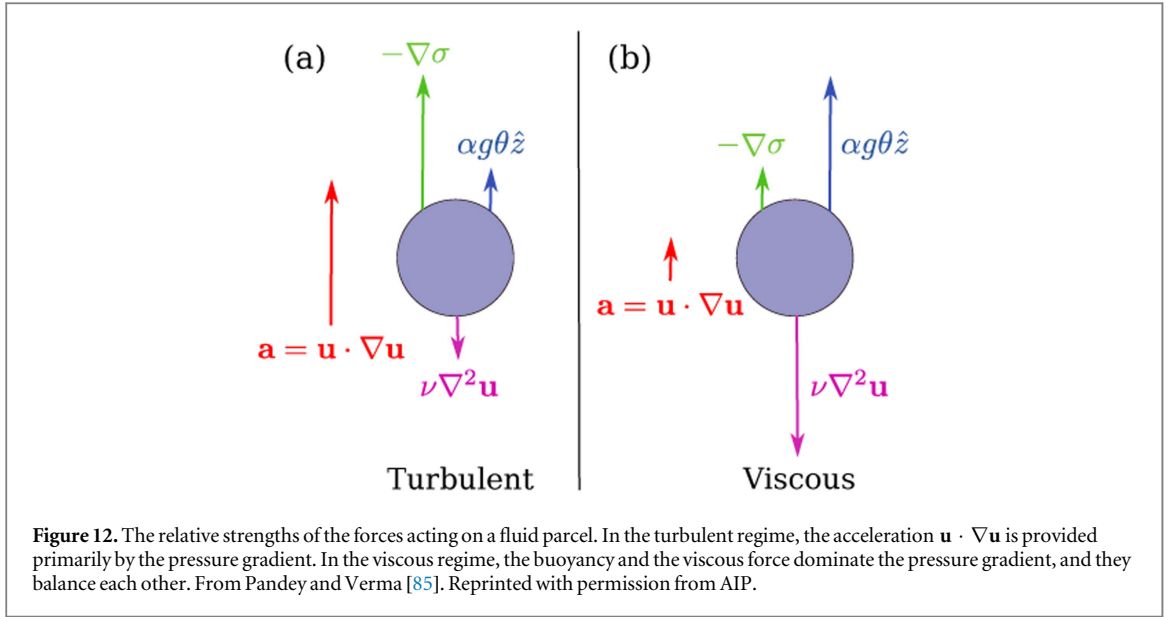
Using the above ideas, GL [38–42, 102] derived the following coupled equations

$$(Nu - 1)RaPr^{-2} = c_1 \frac{Re^2}{g(\sqrt{Re_L}/Re)} + c_2 Re^3, \quad (91)$$

$$Nu - 1 = c_3 \sqrt{RePr} \left\{ f \left[\frac{2aNu}{\sqrt{Re_L}} g \left(\sqrt{\frac{Re_L}{Re}} \right) \right] \right\}^{1/2} + c_4 RePr f \left[\frac{2aNu}{\sqrt{Re_L}} g \left(\sqrt{\frac{Re_L}{Re}} \right) \right], \quad (92)$$

where c_i 's and Re_L are constants, and the functions f and g model the thermal BL [102]. Using the above formulae, GL computed the Nusselt and Reynolds numbers as a function of Ra and Pr that agree with presently available experimental and numerical simulation results quite well [2].

In the next subsection we describe a new model developed recently by Pandey *et al* [84] and Pandey and Verma [85].



4.2. An alternate derivation of Péclet number

Recently Pandey *et al* [84] and Pandey and Verma [85] provided an alternate derivation of Péclet number. Note that $Pe = RePr$. Pandey *et al* [84] analysed the rms values of various terms of the momentum equation, which are exhibited in the schematic diagram of figure 12. Under statistical steady state ($\langle \partial \mathbf{u} / \partial t \rangle \approx 0$), Pandey *et al* observed that in the turbulent regime, the acceleration $\mathbf{u} \cdot \nabla \mathbf{u}$ is primarily provided by the pressure gradient $-\nabla \sigma$, and the buoyancy and viscous terms are relatively small. The above features are consistent with similarities between the turbulence in RBC and hydrodynamics (see section 3.3.2). However, in the viscous regime ($Re \lesssim 1$), $-\nabla \sigma$ is small, and the buoyancy and viscous terms cancel each other resulting in a very small acceleration of the fluid.

Dimensional analysis of the momentum equation yields

$$c_1 \frac{U^2}{d} = c_2 \frac{U^2}{d} + c_3 \alpha g \Delta - c_4 \nu \frac{U}{d^2}, \quad (93)$$

where c_i 's are dimensionless coefficients defined as

$$c_1 = \frac{|\mathbf{u} \cdot \nabla \mathbf{u}|}{U^2/d}; \quad c_2 = \frac{|\nabla \sigma|_{\text{res}} / \rho_m}{U^2/d}; \quad c_3 = |\theta_{\text{res}} / \Delta|; \quad c_4 = \frac{|\nabla^2 \mathbf{u}|}{U/d^2}. \quad (94)$$

Pandey *et al* [84] observed c_i 's to be functions of Ra and Pr that yields interesting and nontrivial scaling relations. It is important to contrast this behaviour with free turbulence (without walls) where c_i 's are constants. Multiplication of equation (93) with d^3/κ^2 yields

$$c_1 Pe^2 = c_2 Pe^2 + c_3 RaPr - c_4 PePr, \quad (95)$$

where $Pe = Ud/\kappa$ is the Péclet number. The solution of the above equation is

$$Pe = \frac{-c_4 Pr + \sqrt{c_4^2 Pr^2 + 4(c_1 - c_2)c_3 RaPr}}{2(c_1 - c_2)}. \quad (96)$$

using which Pe can be computed as a function of Ra and Pr .

In the turbulent regime, the viscous term of equation (95) can be ignored, hence

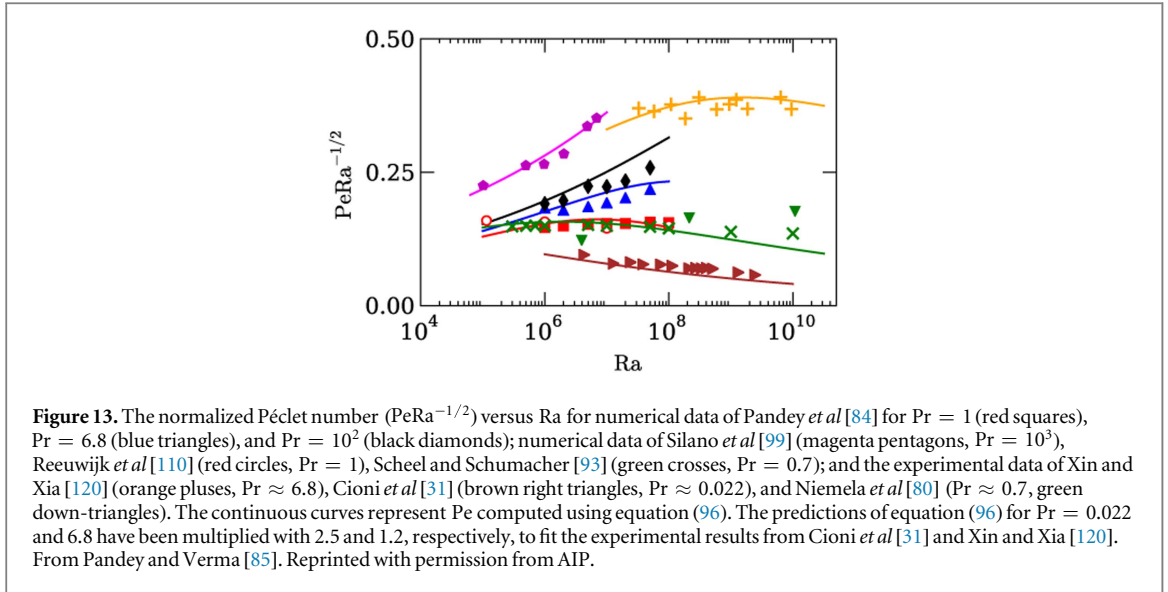
$$Pe \approx \sqrt{\frac{c_3}{|c_1 - c_2|} RaPr}. \quad (97)$$

This limit is applicable when

$$c_4^2 Pr^2 \ll 4|c_1 - c_2|c_3 RaPr. \quad (98)$$

The scaling for the viscous regime is obtained by equating the buoyancy and viscous terms of the momentum equation that yields

$$Pe \approx \frac{c_3}{c_4} Ra. \quad (99)$$



Pandey *et al* [84] computed c_i 's using the RBC simulation data for $Pr = 1, 6.8, 10^2, 10^3$ and Ra from 10^6 to 5×10^8 . These simulations were performed for no-slip boundary condition at all the walls using a finite volume solver OPENFOAM [82]. They reported the following functional form for c_i 's

$$c_1 = 1.5Ra^{0.10}Pr^{-0.06}, \quad (100)$$

$$c_2 = 1.6Ra^{0.09}Pr^{-0.08}, \quad (101)$$

$$c_3 = 0.75Ra^{-0.15}Pr^{-0.05}, \quad (102)$$

$$c_4 = 20Ra^{0.24}Pr^{-0.08}. \quad (103)$$

The errors in the above exponents are $\lesssim 0.01$, except for the Ra exponent of c_4 that has error of the order of 0.10 . In figure 13, we plot the normalized Péclet number, $PeRa^{-1/2}$ for $Pr = 1, 6.8, 10^2$ and compare them with the predictions using equation (96). The figure also exhibits Pe from other simulations and experiments. The plots reveal that the predictions of Pandey *et al* [84] (equation (96)) match with the numerical and experimental results quite well.

Using the above c_i 's and equation (98), we find that $Ra \gg 10^6 Pr$ belongs to the turbulent regime, whereas $Ra \ll 10^6 Pr$ belongs to the viscous regime. In the viscous regime

$$Pe = \frac{c_3}{c_4}Ra \approx 0.038Ra^{0.60}, \quad (104)$$

which is independent of Pr , consistent with the results of Silano *et al* [99], Horn *et al* [46], and Pandey *et al* [86]. For the turbulent regime, equation (97) yields

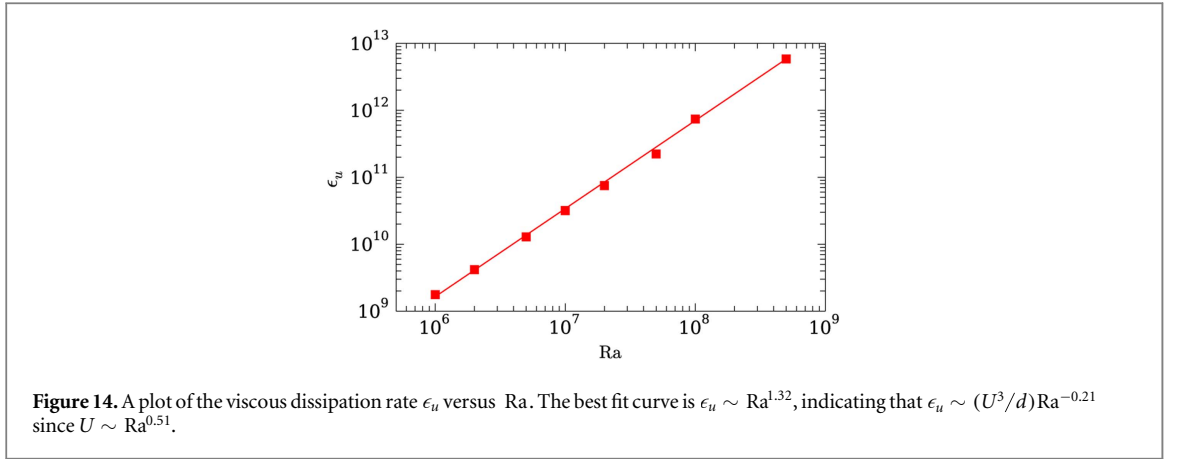
$$Pe = \sqrt{\frac{c_3}{|c_1 - c_2|}} \sqrt{RaPr} \approx \sqrt{7.5 Pr} Ra^{0.38}. \quad (105)$$

For mercury ($Pr \approx 0.025$) as an experimental fluid, Cioni *et al* [31] observed that $Re \sim Ra^{0.424}$, which is close to the predicted exponent of 0.38 discussed above. The range of Rayleigh numbers in the experiment of Cioni *et al* [31] is $5 \times 10^6 \leq Ra \leq 5 \times 10^9$ that is consistent with the turbulent regime estimated above ($Ra \gg 10^6 Pr$). The aforementioned results are in general agreement with those of Grossmann and Lohse [38–42].

4.3. Scaling of Nusselt number and dissipation rates

We revisit the Nusselt number scaling that has been studied widely using theoretical models, experiments, and numerical simulations. The predictions of Grossman and Lohse [38–42], equations (91), (92), fits with the experimental and numerical data quite well. As described earlier, a major debate is whether ultimate regime (exponent = $1/2$) exists or not. See reviews for details [2, 8, 29, 63, 98].

Here we report recent results on the correlation function of equation (88) and the viscous dissipation rate that yield interesting insights. Verma *et al* [116], Pandey *et al* [84], and Pandey and Verma [85] computed $C_{u\theta_{res}}$ of equation (88) for a range of Ra in the turbulent regime and observed nontrivial scaling. They observed that $C_{u\theta_{res}}$, and the rms values of u'_z and θ'_{res} scale with Ra in such a way that $Nu \sim Ra^{0.30}$; without these corrections, $Nu \sim Ra^{1/2}$ in the turbulent regime. Thus, one way to explain the deviation of the exponent from $1/2$ in the ultimate regime [52] is due to the nontrivial scaling of $C_{u\theta_{res}}$, u'_z , and θ'_{res} .



In hydrodynamic turbulence, the viscous dissipation rate $\epsilon_u \approx U^3/d$. However this is not the case in RBC, primarily due to walls or boundary layers. Using numerical data, Verma *et al* [116] and Pandey *et al* [84] have shown that $\epsilon_u \sim Ra^{1.32}$ or

$$\epsilon_u \sim (U^3/d)Ra^{-0.21}. \quad (106)$$

See figure 14 for illustration for $Pr = 1$. One of the exact relations of Shraiman and Siggia [97] yields

$$\epsilon_u = \frac{U^3 (Nu - 1) Ra Pr}{d Pe^3}. \quad (107)$$

Substitution of $Pe \sim Ra^{0.51}$ and $\epsilon_u \sim (U^3/d)Ra^{-0.21}$ yields $Nu \sim Ra^{0.32}$. These arguments show that the reduction of the viscous dissipation rate could be a reason for the deviation of the observed scaling $Nu \sim Ra^{0.32}$ from $Nu \sim Ra^{1/2}$ corresponding to the ultimate regime.

Ni *et al* [77, 78] computed the local (bulk) energy dissipation rate in RBC cell using experimental measurements. They showed that

$$\epsilon_{u,\text{bulk}} \sim \frac{U^3}{d} \sim Ra^{3/2}, \quad (108)$$

which is consistent with the predictions of Grossmann and Lohse [38–42]. Thus the variation of the exponent from the aforementioned $3/2$ to 1.32 of figure 14 is possibly due to the effects of the boundary layers near the walls (also see Pandey and Verma [85]). We require detailed experimental and numerical analysis to resolve this issue.

5. Large-scale flow structures and flow reversals in RBC

The flow properties in the last two sections are related to the random nature of the flow. It has been observed that coherent structures too play important role in the convective flow, and they have certain universal properties. An interesting phenomena of RBC related to large-scale structures is *flow reversals*. Sreenivasan *et al* [101], Brown and Ahlers [16], Xi and Xia [118], and Sugiyama *et al* [103] observed that the vertical velocity near the lateral wall switches sign randomly. Deciphering how the reversals take place is an interesting puzzle, and it is not yet fully solved. In this section we briefly describe the present status of the field.

It is believed that the flow reversals are caused by the nonlinear interaction among the large-scale structures of the flow. For a closed cartesian box, these structures can be conveniently described by the small-wavenumber Fourier modes [21, 22]. This description is useful even for no-slip boundary conditions since the flow structures inside the boundary layers contribute to the large wavenumber modes. For a cylindrical geometry, partial information about the flow structures can be obtained by computing the azimuthal Fourier modes corresponding to the velocity field measured at various angles near the later walls [16, 71, 118]. Here we summarise the main results on the properties of flow reversals.

- (i) During a reversal, the amplitude of the most dominant large-scale mode vanishes, while that of the secondary mode rises sharply. Chandra and Verma [21, 22] reported that during a reversal in a unit two-dimensional cartesian box, the Fourier mode (1, 1) vanishes, while the mode (2, 2), corresponding to the corner rolls, become the most dominant mode [21, 22]. See figure 1 of Chandra and Verma [21]. This numerical result is consistent with the experimental results of Sugiyama *et al* [103].

- (ii) The nature of dominant structures depends on the box geometry and boundary conditions. For example, for a box of size 2×1 , under the no-slip boundary condition, (2, 1) and (2, 2) are the primary and secondary modes respectively. However, under the free-slip boundary condition, the corresponding modes are (1, 1) and (2, 1) respectively [15, 113]; here (3, 1) too plays a major role.
- (iii) Sugiyama *et al* [103], Chandra and Verma [21, 22] and Verma *et al* [113] reported that the flow reversals in two-dimensional turbulent convection are suppressed at large Rayleigh numbers. This is primarily due to relative strengthening of the primary mode (1, 1) compared to the secondary modes. At large Ra, the secondary modes become too weak to be able to cause flow reversals.
- (iv) Huang *et al* [47] studied the flow reversals for two different boundary conditions: (a) constant temperatures at both the boundaries (CTCT), and (b) constant heat flux at the bottom plate and constant temperature at the top plate (CFCT). They showed that the flow reversals are more frequent in the CTCT case compared to the CFCT case despite the former being more stable than the latter. Thus, the flow reversals are not directly related to the flow instability [47].
- (v) Verma *et al* [113] have constructed a group-theoretic argument to decipher the reversing and non-reversing modes during a reversals. The structure of the groups is related to the Klein group.
- (vi) Thermal convection in a cylinder exhibit reversals that have similar behaviour as above. Brown and Ahlers [16] termed such reversals as *cessation-led reversals*. Note however that during a cessation-led reversal, the secondary modes become significant, hence the kinetic energy does not vanish.
- (vii) Cylindrical convection exhibits another kind of flow reversals, called *rotation-led reversals*, in which the large-scale structure rotates azimuthally [16, 71, 118]. This rotation is due to the azimuthal rotation symmetry of the system. Such phenomena is also observed in a cylindrical annulus [76].

These observations reinforce the viewpoint that the nonlinear interactions among the large-scale structure are very relevant for flow reversals. The magnetic field reversals in dynamo [36], and the velocity field reversals in Kolmogorov-flow [74] also involve nonlinear interactions among the large-scale structures of the flow. Thus, these reversals share certain similarities with the flow reversals of RBC.

6. Summary

In this paper we describe the recent results on the spectral and large-scale properties of buoyancy-driven turbulence—stably-stratified flows and RBC. A summary of the results covered in this review is as follows:

- (i) The SST is nearly isotropic for Froude number $Fr \gtrsim 1$. Bolgiano [11] and Obukhov [81] showed that for gravity-dominated flows ($Fr \approx 1$), the kinetic-energy spectrum $E_u(k) \sim k^{-11/5}$. Kumar *et al* [53] demonstrated this scaling using numerical simulations.
- (ii) For $Fr \gg 1$, SST exhibits Kolmogorov scaling, i.e. $E_u(k) \sim k^{-5/3}$, due to the dominance of the nonlinear term over the buoyancy.
- (iii) For $Fr \ll 1$, SST is quasi two-dimensional, and the kinetic-energy spectrum exhibits a combination of $k^{-5/3}$ and k^{-3} . We do not discuss this case in detail. We refer the reader to Lindborg [60], Brethouwer *et al* [14], and Bartello and Tobias [4].
- (iv) In three dimensions and for Prandtl number $\lesssim 1$, turbulence in RBC has strong similarities with the hydrodynamic turbulence, e.g. it exhibits constant energy flux and $k^{-5/3}$ energy spectrum in the inertial range. For very large and infinite Prandtl numbers, convective turbulence has $E_u(k) \sim k^{-13/3}$. The energy spectrum is expected to be different in two dimensions and in the boundary layer.
- (v) In RBC turbulence, the pressure gradient accelerates the flow, while the buoyancy is balanced by the viscous dissipation. This observation is consistent with the Kolmogorov-like phenomenology observed for RBC.
- (vi) The aforementioned phenomenology of RBC turbulence is expected to work for other buoyancy-driven flows in which buoyancy feeds the kinetic energy. Some of the examples of such flows are bubbly turbulence, non-Boussinesq thermally-driven flows in stars, turbulent buoyancy-driven exchange flows in a vertical pipe [3], etc.

- (vii) The scaling of the Reynolds and Nusselt numbers of RBC are well described by the models of Grossmann and Lohse [38–42]. Recently Pandey *et al* [84] and Pandey and Verma [85] derived a formula for the Péclet number that fits with the experimental and numerical data quite well.

In a short review it is impossible to cover the vast number of results of buoyancy-driven turbulence. Here we could not describe recent results on the ultimate regime of turbulent convection [44, 107], logarithmic profile of the boundary layer [96, 108], new scaling of temperature [45], rotating convection [23], etc. Also we could not discuss SST for $Fr \ll 1$, which is very important for atmospheric turbulence. We hope that a more comprehensive review will be written. For relatively older works, we refer the reader to the review articles [2, 8, 29, 63, 98].

In this article we covered the present status of the energy spectrum and flux of turbulent convection that shows certain resolution. The issue of Nusselt number exponent being $1/2$ or ≈ 0.3 , and the existence of the ultimate regime is being intensely investigated. The structure and dynamics of boundary layer (e.g. existence of log layer or not), flow reversals, and intermittency in RBC are also of major interest. High-resolution simulations, advanced experiments, and careful modelling may resolve these outstanding questions in future.

Acknowledgments

We thank Stephan Fauve, Jörg Schumacher, Pankaj Mishra, Ravi Samtaney, Mani Chandra, Supriyo Paul, Anando Chatterjee, and Jayant Bhattacharjee for valuable discussions. Our numerical simulations were performed on Cray XC40 ‘Shaheen II’ at KAUST supercomputing laboratory, Saudi Arabia. This work was supported by the research grants SERB/F/3279 from Science and Engineering Research Board, India, and PLANEX/PHY/2015239 from Indian Space Research Organisation, India.

References

- [1] Ahlers G, Dressel B, Oh J and Pech W 2010 Strong non-Boussinesq effects near the onset of convection in a fluid near its critical point *J. Fluid Mech.* **642** 15–48
- [2] Ahlers G, Grossmann S and Lohse D 2009 Heat transfer and large scale dynamics in turbulent Rayleigh–Bénard convection *Rev. Mod. Phys.* **81** 503–37
- [3] Arakeri J H, Avila F E, Dada J M and Tovar R O 2000 Convection in a long vertical tube due to unstable stratification—a new type of turbulent flow? *Curr. Sci.* **79** 859–66
- [4] Bartello P and Tobias S M 2013 Sensitivity of stratified turbulence to the buoyancy Reynolds number *J. Fluid Mech.* **725** 1–22
- [5] Bhattacharjee J K 1987 *Convection and Chaos in Fluids* (Singapore: World Scientific)
- [6] Bhattacharjee J K 2015 Kolmogorov argument for the scaling of the energy spectrum in a stratified fluid *Phys. Lett. A* **379** 696–9
- [7] Bhattacharjee J K 2015 Self-consistent field theory for the convective turbulence in a Rayleigh–Bénard system in the infinite Prandtl number limit *J. Stat. Phys.* **160** 1519–28
- [8] Bodenschatz E, Pesch W and Ahlers G 2000 Recent developments in Rayleigh–Bénard convection *Ann. Rev. Fluid Mech.* **32** 709–78
- [9] Boffetta G, De Lillo F, Mazzino A and Musacchio S 2011 Bolgiano scale in confined Rayleigh–Taylor turbulence *J. Fluid Mech.* **690** 426–40
- [10] Boffetta G, Mazzino A, Musacchio S and Vozella L 2009 Kolmogorov scaling and intermittency in Rayleigh–Taylor turbulence *Phys. Rev. E* **79** 065301
- [11] Bolgiano R 1959 Turbulent spectra in a stably stratified atmosphere *J. Geophys. Res.* **64** 2226–9
- [12] Borue V and Orszag S A 1997 Turbulent convection driven by a constant temperature gradient *J. Sci. Comput.* **12** 305–51
- [13] Brandenburg A 1992 Energy-spectra in a model for convective turbulence *Phys. Rev. Lett.* **69** 605
- [14] Brethouwer G, Billant P, Lindborg E and Chomaz J-M 2007 Scaling analysis and simulation of strongly stratified turbulent flows *J. Fluid Mech.* **585** 343–68
- [15] Breuer M and Hansen U 2009 Turbulent convection in the zero Reynolds number limit *Eur. Phys. Lett.* **86** 24004
- [16] Brown E and Ahlers G 2006 Rotations and cessations of the large-scale circulation in turbulent Rayleigh–Bénard convection *J. Fluid Mech.* **568** 351–86
- [17] Busse F H and Clever R M 1978 Asymmetric squares as an attracting set in Rayleigh–Bénard convection *Phys. Rev. Lett.* **81** 341
- [18] Calzavarini E, Lohse D and Toschi F 2005 Rayleigh and Prandtl number scaling in the bulk of Rayleigh–Bénard turbulence *Phys. Fluids* **17** 055107
- [19] Calzavarini E, Toschi F and Tripiccione R 2002 Evidences of Bolgiano–Obukhov scaling in three-dimensional Rayleigh–Bénard convection *Phys. Rev. E* **66** 016304
- [20] Camussi R and Verzicco R 2004 Temporal statistics in high Rayleigh number convective turbulence *Eur. J. Mech.* **B 23** 427–42
- [21] Chandra M and Verma M K 2011 Dynamics and symmetries of flow reversals in turbulent convection *Phys. Rev. E* **83** 067303
- [22] Chandra M and Verma M K 2013 Flow reversals in turbulent convection via vortex reconnections *Phys. Rev. Lett.* **110** 114503
- [23] Chandrasekhar S 1968 *Hydrodynamic and Hydromagnetic Stability* (Oxford: Clarendon)
- [24] Chertkov M 2003 Phenomenology of Rayleigh–Taylor turbulence *Phys. Rev. Lett.* **91** 115001
- [25] Chilla F, Ciliberto S, Innocenti C and Pampaloni E 1993 Boundary layer and scaling properties in turbulent thermal convection *Nuovo Cimento D* **15** 1229
- [26] Chilla F and Schumacher J 2012 New perspectives in turbulent Rayleigh–Bénard convection *Eur. Phys. J. E* **35** 58
- [27] Ching E S C 2007 Scaling laws in the central region of confined turbulent thermal convection *Phys. Rev. E* **75** 056302
- [28] Ching E S C and Cheng W C 2008 Anomalous scaling and refined similarity of an active scalar in a shell model of homogeneous turbulent convection *Phys. Rev. E* **77** 015303

- [29] Ching E S C 2014 *Statistics and Scaling in Turbulent Rayleigh-Bénard Convection* (Singapore: Springer)
- [30] Cioni S, Ciliberto S and Sommeria J 1995 Temperature structure functions in turbulent convection at low Prandtl number *Eur. Phys. Lett.* **32** 413–8
- [31] Cioni S, Ciliberto S and Sommeria J 1997 Strongly turbulent Rayleigh-Bénard convection in mercury: comparison with results at moderate Prandtl number *J. Fluid Mech.* **335** 111–40
- [32] Dar G, Verma M K and Eswaran V 2001 Energy transfer in two-dimensional magnetohydrodynamic turbulence: formalism and numerical results *Physica D* **157** 207–25
- [33] DeDominicis C and Martin P C 1979 Energy spectra of certain randomly-stirred fluids *Phys. Rev. A* **19** 419
- [34] Emran M S and Schumacher J 2008 Fine-scale statistics of temperature and its derivatives in convective turbulence *J. Fluid Mech.* **611** 13–34
- [35] Gage K S and Nastrom G D 1986 Theoretical interpretation of atmospheric wavenumber spectra of wind and temperature observed by commercial aircraft during GASP *J. Atmos. Sci.* **43** 729–40
- [36] Gallet B, Herault J, Laroche C, Pétrélis F and Fauve S 2012 Reversals of a large-scale field generated over a turbulent background *Geophys. Astrophys. Fluid Dyn.* **106** 468–92
- [37] Grossmann S and Lohse D 1991 Fourier-Weierstrass mode analysis for thermally driven turbulence *Phys. Rev. Lett.* **67** 445
- [38] Grossmann S and Lohse D 2000 Scaling in thermal convection: a unifying theory *J. Fluid Mech.* **407** 27–56
- [39] Grossmann S and Lohse D 2001 Thermal convection for large Prandtl numbers *Phys. Rev. Lett.* **86** 3316
- [40] Grossmann S and Lohse D 2002 Prandtl and Rayleigh number dependence of the Reynolds number in turbulent thermal convection *Phys. Rev. E* **66** 016305
- [41] Grossmann S and Lohse D 2004 Fluctuations in turbulent Rayleigh-Bénard convection: the role of plumes *Phys. Fluids* **16** 4462–72
- [42] Grossmann S and Lohse D 2011 Multiple scaling in the ultimate regime of thermal convection *Phys. Fluids* **23** 045108
- [43] Grossmann S, Lohse D and Sun C 2016 High-Reynolds number Taylor-Couette turbulence *Annu. Rev. Fluid Mech.* **48** 53–80
- [44] He X, Fufschilling D, Nobach H, Bodenschatz E and Ahlers G 2012 Transition to the ultimate state of turbulent Rayleigh-Bénard convection *Phys. Rev. Lett.* **108** 024502
- [45] He X, van Gils D P M, Bodenschatz E and Ahlers G 2014 Logarithmic spatial variations and universal f^{-1} power spectra of temperature fluctuations in turbulent Rayleigh-Bénard convection *Phys. Rev. Lett.* **112** 174501
- [46] Horn S, Shishkina O and Wagner C 2013 On Oberbeck-non-Boussinesq effects in three-dimensional Rayleigh-Bénard convection in glycerol *J. Fluid Mech.* **724** 175–202
- [47] Huang S-D, Wang F, Xi H-D and Xia K-Q 2015 Comparative experimental study of fixed temperature and fixed heat flux boundary conditions in turbulent thermal convection *Phys. Rev. Lett.* **115** 154502
- [48] Kaczorowski M and Xia K-Q 2013 Turbulent flow in the bulk of Rayleigh-Bénard convection: small-scale properties in a cubic cell *J. Fluid Mech.* **722** 596–617
- [49] Kerr R M 1996 Rayleigh number scaling in numerical convection *J. Fluid Mech.* **310** 139–79
- [50] Kolmogorov A N 1941 The local structure of turbulence in incompressible viscous fluid for very large Reynolds numbers *Dokl. Akad. Nauk. SSSR* **30** 301–5
- [51] Kraichnan R H 1959 The structure of isotropic turbulence at very high Reynolds numbers *J. Fluid Mech.* **5** 497–543
- [52] Kraichnan R H 1962 Turbulent thermal convection at arbitrary Prandtl number *Phys. Fluids* **5** 1374
- [53] Kumar A, Chatterjee A G and Verma M K 2014 Energy spectrum of buoyancy-driven turbulence *Phys. Rev. E* **90** 023016
- [54] Kumar A and Verma M K 2015 Shell model for buoyancy-driven turbulence *Phys. Rev. E* **91** 043014
- [55] Kumar A and Verma M K 2015 Shell model for buoyancy-driven turbulent flows *Proc. Advances in Computation, Modeling and Control of Transitional and Turbulent Flows* ed T K Sengupta, et al pp 232–41
- [56] Kumar A and Verma M K 2016 Applicability of Taylor's hypothesis in convective turbulence arXiv:1512.00959
- [57] Kunnen R P J, Clercx H J H, Geurts B J, van Bokhoven L J A, Akkermans R A D and Verzicco R 2008 Numerical and experimental investigation of structure-function scaling in turbulent Rayleigh-Bénard convection *Phys. Rev. E* **77** 016302
- [58] Lesieur M 2012 *Turbulence in Fluids* 4th edn (Dordrecht: Springer)
- [59] Leslie D C 1973 *Developments in the Theory of Turbulence* (Oxford: Clarendon)
- [60] Lindborg E 2006 The energy cascade in a strongly stratified fluid *J. Fluid Mech.* **550** 207–42
- [61] Lindborg E and Brethouwer G 2008 Vertical dispersion by stratified turbulence *J. Fluid Mech.* **614** 303–14
- [62] Lohse D and Toschi F 2003 Ultimate state of thermal convection *Phys. Rev. Lett.* **90** 034502
- [63] Lohse D and Xia K-Q 2010 Small-scale properties of turbulent Rayleigh-Bénard convection *Annu. Rev. Fluid Mech.* **42** 335–64
- [64] Lozhkin S A and Frick P G 1998 Inertial Obukhov-Bolgiano interval in shell models of convective turbulence *Fluid Dyn.* **33** 842–9
- [65] L'vov V S 1991 Spectra of velocity and temperature-fluctuations with constant entropy flux of fully-developed free-convective turbulence *Phys. Rev. Lett.* **67** 687
- [66] L'vov V S and Falkovich G 1992 Conservation laws and two-flux spectra of hydrodynamic convective turbulence *Physica D* **57** 85–95
- [67] Manneville P 2004 *Instabilities, Chaos, and Turbulence* (London: Imperial College Press)
- [68] McComb W D 1990 *The Physics of Fluid Turbulence* (Oxford: Clarendon)
- [69] McComb W D and Shanmugasundaram V 1985 Renormalisation group calculation of the eddy viscosity for isotropic turbulence *J. Phys. A: Math. Theor.* **18** 2191–8
- [70] Mingshun J and Shida L 1997 Scaling behavior of velocity and temperature in a shell model for thermal convective turbulence *Phys. Rev. E* **56** 441
- [71] Mishra P K, De A K, Verma M K and Eswaran V 2010 Dynamics of reorientations and reversals of large-scale flow in Rayleigh-Bénard convection *J. Fluid Mech.* **668** 480–99
- [72] Mishra P K and Verma M K 2010 Energy spectra and fluxes for Rayleigh-Bénard convection *Phys. Rev. E* **81** 056316
- [73] Mishra P K, Wahi P and Verma M K 2010 Patterns and bifurcations in low-Prandtl-number Rayleigh-Bénard convection *Eur. Phys. Lett.* **89** 44003
- [74] Mishra P K, Herault J, Fauve S and Verma M K 2015 Dynamics of reversals and condensates in two-dimensional Kolmogorov flows *Phys. Rev. E* **91** 053005
- [75] Nath D, Pandey A, Kumar A and Verma M K 2016 Near isotropic behaviour of turbulent thermal convection *Phys. Rev. Fluids* **1** 064302
- [76] Nath D and Verma M K 2014 Numerical simulation of convection of argon gas in fast breeder reactor *Ann. Nucl. Energy* **63** 51–8
- [77] Ni R, Huang S-D and Xia K-Q 2011 Local energy dissipation rate balances local heat flux in the center of turbulent thermal convection *Phys. Rev. Lett.* **107** 174503
- [78] Ni R, Huang S-D and Xia K-Q 2012 Lagrangian acceleration measurements in convective thermal turbulence *J. Fluid Mech.* **692** 395–419

- [79] Niemela J J, Skrbek L, Sreenivasan K R and Donnelly R J 2000 Turbulent convection at very high Rayleigh numbers *Nature* **404** 837
- [80] Niemela J J, Skrbek L, Sreenivasan K R and Donnelly R J 2001 The wind in confined thermal convection *J. Fluid Mech.* **449** 169–78
- [81] Obukhov A M 1959 On influence of buoyancy forces on the structure of temperature field in a turbulent flow *Dokl. Acad. Nauk. SSSR* **125** 1246
- [82] OpenFOAM. *The open source CFD toolbox*, www.openfoam.org, 2015
- [83] Pal P, Wahi P, Paul S, Verma M K, Kumar K and Mishra P K 2009 Bifurcation and chaos in zero-Prandtl-number convection *Eur. Phys. Lett.* **87** 54003
- [84] Pandey A, Kumar A, Chatterjee A G and Verma M K 2016 Dynamics of large-scale quantities in Rayleigh–Bénard convection *Phys. Rev. E* **94** 053106
- [85] Pandey A and Verma M K 2016 Scaling of large-scale quantities in Rayleigh–Bénard convection *Phys. Fluids* **28** 095105
- [86] Pandey A, Verma M K and Mishra P K 2014 Scaling of heat flux and energy spectrum for very large Prandtl number convection *Phys. Rev. E* **94** 053106
- [87] Pawar S S and Arakeri J H 2016 Kinetic energy and scalar spectra in high Rayleigh number axially homogeneous buoyancy driven turbulence *Phys. Fluids* **28** 065103
- [88] Prakash V N, Martínez Mercado J, van Wijngaarden L, Mancilla E, Tagawa Y, Lohse D and Sun C 2016 Energy spectra in turbulent bubbly flows *J. Fluid Mech.* **791** 174–90
- [89] Procaccia I and Zeitak R 1989 Scaling exponents in nonisotropic convective turbulence *Phys. Rev. Lett.* **62** 2128
- [90] Riley J J and Lindborg E 2013 Recent progress in stratified turbulence *Ten Chapters in Turbulence* ed P A Davidson et al (Cambridge: Cambridge University Press) pp 269–312
- [91] Rubinstein R 1994 Renormalization group theory of Bolgiano scaling in Boussinesq turbulence *NASA Technical Memorandum* 106602, ICOMP-94-8; CMOTT-94-2
- [92] Sameen A, Verzicco R and Sreenivasan K R 2009 Specific roles of fluid properties in non-Boussinesq thermal convection at the Rayleigh number of 2×10^8 *Eur. Phys. Lett.* **86** 14006
- [93] Scheel J D and Schumacher J 2014 Local boundary layer scales in turbulent Rayleigh–Bénard convection *J. Fluid Mech.* **758** 344–73
- [94] Shang X-D and Xia K-Q 2001 Scaling of the velocity power spectra in turbulent thermal convection *Phys. Rev. E* **64** 65301
- [95] Shishkina O and Thess A 2009 Mean temperature profiles in turbulent Rayleigh–Bénard convection of water *J. Fluid Mech.* **633** 449
- [96] Shishkina O, Horn S and Wagner S 2015 Thermal boundary layer equation for turbulent Rayleigh–Bénard convection *Phys. Rev. Lett.* **114** 114302
- [97] Shraiman B I and Siggia E D 1990 Heat transport in high-Rayleigh-number convection *Phys. Rev. A* **42** 3650–3
- [98] Siggia E D 1994 High Rayleigh number convection *Annu. Rev. Fluid Mech.* **26** 137–68
- [99] Silano G, Sreenivasan K R and Verzicco R 2010 Numerical simulations of Rayleigh–Bénard convection for Prandtl numbers between 10^{-1} and 10^4 and Rayleigh numbers between 10^5 and 10^9 *J. Fluid Mech.* **662** 409–46
- [100] Škandera D, Busse A and Müller W C 2008 Scaling properties of convective turbulence *High Performance Computing in Science and Engineering, Transactions of the Third Joint HLRB and KONWIHR Status and Result Workshop* (Berlin: Springer) p 387 Part IV
- [101] Sreenivasan K R, Bershadskii A and Niemela J J 2002 Mean wind and its reversal in thermal convection *Phys. Rev. E* **65** 056306
- [102] Stevens R, Poel E P, Grossmann S and Lohse D 2013 The unifying theory of scaling in thermal convection: the updated prefactors *J. Fluid Mech.* **730** 295–308
- [103] Sugiyama K, Ni R, Stevens R J A M, Chan T-S, Zhou S-Q, Xi H-D, Sun C, Grossmann S, Xia K-Q and Lohse D 2010 Flow reversals in thermally driven turbulence *Phys. Rev. Lett.* **105** 034503
- [104] Sun C, Zhou Q and Xia K-Q 2006 Cascades of velocity and temperature fluctuations in buoyancy-driven thermal turbulence *Phys. Rev. Lett.* **97** 144504
- [105] Taylor G I 1938 The spectrum of turbulence *Proc. R. Soc. A* **164** 476
- [106] Toh S and Suzuki E 1994 Entropy cascade and energy inverse transfer in two-dimensional convective turbulence *Phys. Rev. Lett.* **73** 1501
- [107] Urban P, Hanzelka P, Kralik T, Musilova V, Srnka A and Skrbek L 2012 Effect of boundary layers asymmetry on heat transfer efficiency in turbulent Rayleigh–Bénard convection at very high Rayleigh numbers *Phys. Rev. Lett.* **109** 154301
- [108] van der Poel E P, Ostilla-Mónico R, Verzicco R, Grossmann S and Lohse D 2015 Logarithmic mean temperature profiles and their connection to plume emissions in turbulent Rayleigh–Bénard convection *Phys. Rev. Lett.* **115** 154501
- [109] Vallgren A, Deusebio E and Lindborg E 2011 Possible explanation of the atmospheric kinetic and potential energy spectra *Phys. Rev. Lett.* **107** 268501
- [110] van Reeuwijk M, Jonker H J J and Hanjalić K 2008 Wind and boundary layers in Rayleigh–Bénard convection: I. Analysis and modeling *Phys. Rev. E* **77** 036311
- [111] Verma M K 2004 Statistical theory of magnetohydrodynamic turbulence: recent results *Phys. Rep.* **401** 229–380
- [112] Verma M K 2012 Variable enstrophy flux and energy spectrum in two-dimensional turbulence with Ekman friction *Eur. Phys. Lett.* **98** 14003
- [113] Verma M K, Ambhire S C and Pandey A 2015 Flow reversals in turbulent convection with free-slip walls *Phys. Fluids* **27** 047102 047102–16
- [114] Verma M K, Kumar A and Chatterjee A G 2015 Energy spectrum and flux of buoyancy-driven turbulence *Proc. Advances in Computation, Modeling and Control of Transitional and Turbulent Flows* ed T K Sengupta et al pp 442–51
- [115] Verma M K, Kumar A and Chatterjee A G 2015 Energy spectrum and flux of buoyancy-driven turbulence *Phys. Focus* **25** 45
- [116] Verma M K, Mishra P K, Pandey A and Paul S 2012 Scalings of field correlations and heat transport in turbulent convection *Phys. Rev. E* **85** 016310
- [117] Verzicco R and Camussi R 2003 Numerical experiments on strongly turbulent thermal convection in a slender cylindrical cell *J. Fluid Mech.* **477** 19–49
- [118] Xi H-D and Xia K-Q 2007 Cessations and reversals of the large-scale circulation in turbulent thermal convection *Phys. Rev. E* **75** 066307
- [119] Xia K Q 2013 Current trends and future directions in turbulent thermal convection *Theor. Appl. Mech. Lett.* **3** 052001
- [120] Xin Y-B and Xia K-Q 1997 Boundary layer length scales in convective turbulence *Phys. Rev. E* **56** 3010
- [121] Yakhot V and Orszag S A 1986 Renormalization group analysis of turbulence: I. Basic theory *J. Sci. Comput.* **1** 3–51
- [122] Zhou Q, Li C M, Lu Z M and Liu Y L 2011 Experimental investigation of longitudinal space-time correlations of the velocity field in turbulent Rayleigh–Bénard convection *J. Fluid Mech.* **683** 94–111
- [123] Zhou Q, Sun C and Xia K Q 2008 Experimental investigation of homogeneity, isotropy, and circulation of the velocity field in buoyancy-driven turbulence *J. Fluid Mech.* **598** 361–72
- [124] Zhou S-Q and Xia K-Q 2001 Scaling properties of the temperature field in convective turbulence *Phys. Rev. Lett.* **87** 64501